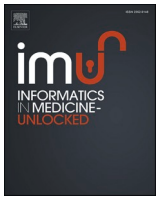
Informatics in Medicine Unlocked 39 (2023) 101261



Contents lists available at ScienceDirect

Informatics in Medicine Unlocked

journal homepage: www.elsevier.com/locate/imu





Identification of neurotherapeutic constituents in *Ocimum gratissimum* with cholinesterase and mono amine oxidase inhibitory activities, using GC-MS analysis, in *vitro,* and *in silico* approaches

Anoka A. Njan [a,*], Esther O. Olaleye [a], Saheed O. Afolabi [a], Immanuel Anoka-Ayembe [b], Gideon A. Gyebi [c], Amase Nyamngee [d], Udoka N. Okeke [a], Solomon O. Olaoye [e], Fortune M. Alabi [f], Oluwapelumi P. Adeleke [a], Hussaini D. Ibrahim [f]

[a] *Department of Pharmacology and Therapeutics, Faculty of Basic Clinical Sciences, College of Health Sciences, University of Ilorin, Ilorin, Nigeria*
[b] *Department of Computer Science, Whitworth University, Spokane, WA, USA*
[c] *Department of Biochemistry, Faculty of Science and Technology, Bingham University, Karu, Nasarawa, State, Nigeria*
[d] *Department of Medicinal Microbiology and Parasitology, Faculty of Basic Clinical Science, College of Health Sciences, University of Ilorin, Ilorin, Nigeria*
[e] *General Hospital Kisi, Oyo State, Nigeria*
[f] *Raw Materials Research and Development Council, Maitama, Abuja, Nigeria*

A R T I C L E I N F O

Keywords:
Ocimum gratissimum
Cholinesterases
Monoamine oxidase
Ensemble-based docking
Clustering analysis
Molecular dynamics

A B S T R A C T

Neuroprotective activities of various extracts of *Ocimum gratissimum (OG),* have been reported, but there is paucity of information on its neurotherapeutic constituents. This study is aimed at identifying the neurotherapeutic constituents in OG leaves using *in vitro* assays, GC-MS chemical investigation and in silico studies including molecular docking, ensemble-based docking, molecular dynamics (MD) simulation, clustering and ADMET filtering analysis. Methanol extract of *O gratissimum* (MEOG) and solvent-partition (n-hexane, ethylacetate, and methanol residue fraction) of MEOG were investigated for *in vitro* acetylcholinesterase (AChE), butyrylcholinesterase (BChE) and monoamine oxidase B (MAO-B) inhibition at concentration of 0.65, 12.5, 2.5, 5, and 10 mg/mL, using donepezil, phenazine methosulfate and selegiline as reference inhibitors for AChE, BChE and MAO B respectively. n-hexane solvent partition fraction was further investigated using GC-MS analysis. Identified compounds were screened against human AChE, BChE and MAO-B activities using molecular docking and molecular dynamics. The lead phytochemicals were further analysed for ADMET in silico analysis. MEOG and the 3 fractions (n-hexane, ethylacetate, and methanol residue fraction) inhibited the activities of AChE, BChE and MAO-B in a concentration-dependent manner with AChE (IC_{50} = 2.380, 2.022, 2.066 and 1.079 mg/mL respectively), BChE (IC_{50} = 2.261, 2.126, 2.630 and 1.465 mg/mL respectively) and MAO-B (IC_{50} = 2.345, 1.584, 2.933 and 2.935 mg/mL respectively). From the 38 GC-MS identified compounds, 7 hit compounds were further subjected to ensemble-docking, the lead phytochemicals (LP): cholestane and 3-methoxy-morphanin presented highest multiple binding tendencies to the three enzymes. Cholestane had the highest binding energies of −9.9, −9.0 and −11 kcal/mol, while 3-methoxy-morphanin presented the second-best binding energies of −9.3, −8.2 and −10.1 kcal/mol respectively. When compared with the binding pattern of reference inhibitors of the enzyme, lead phytochemicals were orientated in the catalytic sites of the enzyme and interacted with important catalytic residues. The LP-enzyme complexes were stable during the MD simulation analysis. Cholestane and 3-methoxy-morphanin presented favorable ADMET properties over several molecular descriptors and filters, with druggable properties and ability to cross the blood-brain barrier. Hence, cholestane and 3-methoxy-morphanin, in part, or in synergy with other hit phytochemicals, may be responsible for the neurotherapeutic activities of MEOG leaves.

* Corresponding author.
E-mail address: anoka.an@unilorin.edu.ng (A.A. Njan).

https://doi.org/10.1016/j.imu.2023.101261
Received 8 March 2023; Received in revised form 1 May 2023; Accepted 2 May 2023
Available online 4 May 2023
2352-9148/© 2023 The Authors. Published by Elsevier Ltd. This is an open access article under the CC BY-NC-ND license (http://creativecommons.org/licenses/by-nc-nd/4.0/).

1. Introduction

Neurodegenerative disorders (NDs) are a broad range of diseases characterized by slow and irreversible damage of neurons and neuronal structures in specific regions of the brain. NDs, including Parkinson's disease (PD), Huntington's disease (HD), Alzheimer's disease (AD), and amyotrophic lateral sclerosis (ALS), have the most devastating effects. The last two disorders involve loss of neuronal structures of the basal ganglia that lead to irregularity in movement coordination [1], while AD, the prevalent form of ND worldwide, is typified by the progressive loss of cognition, memory, and learning due to loss of cortical and hippocampal neurons [2] and is projected to triple by 2050 [3]. Several etiological factors are linked to the development of NDs, including the deposition of metal ions, with the consequence of altering the biochemical homeostasis of the nervous system, disturbance in cholinesterase and monoamine oxidase (MAO), oxidative stress, formation of amyloid and tau plaque, and loss of dopaminergic neurons and dopamine [4–6]. One of the major hallmarks of imbalance and neurochemical disturbances in AD is the deficit in acetylcholine levels. Hence, the enhancement of cholinergic transmission is presently the basis of AD treatment [7], and inhibition of enzymes involved in hydrolysis of the neurotransmitter could enhance cholinergic transmission [8].

However, several licensed drugs for the management ofAD, such as galantamine, rivastigmine, and donepezil, which work through their inhibitory action cholinesterases, have been reported to cause several adverse effects including tiredness muscle cramps, vomiting, diarrhea, insomnia, and nausea [7]. On the other hand, NDs such as PD are defined by the loss of the dopaminergic neuron and dopamine, and one of the approaches used to maintain the levels of required dopamine in the substantial nigra pars compacta is inhibition of monoamine oxidase (MAO). MAO is responsible for catalyzing the oxidative deamination of dopamine; this mechanism has been considered to be a plausible means of decreasing levels in the dopamine stratum [9,10]. Considering the undesirable effect of conventional drugs for the management of NDs, dietary sources of cholinesterase inhibitors, especially from food plants with no or minimal toxicity, could be an alternative approach for the prevention/management of these diseases. Compounds that can offer inhibitory activities against both AChE and BChE are often desired over selective inhibitors of enzymes in neurodegenerative diseases such as AD, BChE represents the main cholinesterase in late-stage AD in humans [11]. Furthermore, inhibition of BChE has been reported to decrease the rate of neurotoxic plaque production, which is a known risk factor in the development of NDs such as AD [12]. Plant-derived medicines are usually prepared from crude plant extracts that include an intricate mixture of several phytochemicals, of which most are secondary metabolites [13], these phytochemicals are made up of unique and complex structures [14]. The identification, isolation, and characterization of these phytocompounds from several plants with medical properties have led to the development of drug candidates with a high activity profile [15]. Gas chromatography mass spectrometry (GC-MS) has been used for rapid and accurate investigation of phytochemicals, including alkaloids, esters, steroids, nitro compounds, long-chain hydrocarbons, alcohols, that are present in plant-based materials [16,17]. Recent advances in the development of several virtual screening software and protein ligand modelling tools coupled with increased protein crystallographic techniques have enhanced the various stages of drug design and development [18]. One of the important tools used in computer-aided drug design is molecular docking simulation because of its ability to predict the interaction of ligand and receptor at the molecular level. This tool has helped identify potential drug candidates at comparatively low cost in a short period of time. The potential drug candidates that are discovered by this model can inform the next line of experimentation, thus reducing the total cost of drug discovery [19]. The result obtained from this simulation analysis can provide a list of promising drug candidates on which wet laboratory experiments can be performed in an informed manner, thus reducing the overall cost of drug discovery [20,21]. The ensemble-based molecular docking approach in which several conformations of the targeted enzymes, usually obtained from MD simulation, has recently been established as a more

Table 1
Binding site coordinates of target proteins.

Dimensions	Monoamine oxidase B (Å)	Acetylcholinesterase (Å)	Butyrlcholinesterase (Å)
center_x	16.84	−13.48	2.54
center_y	129.50	−43.40	−9.30
center_z	22.92	27.61	−14.86
Size x	18.99	24.78	18.53
Size y	17.99	16.73	21.94
Size z	19.87	17.05	20.98

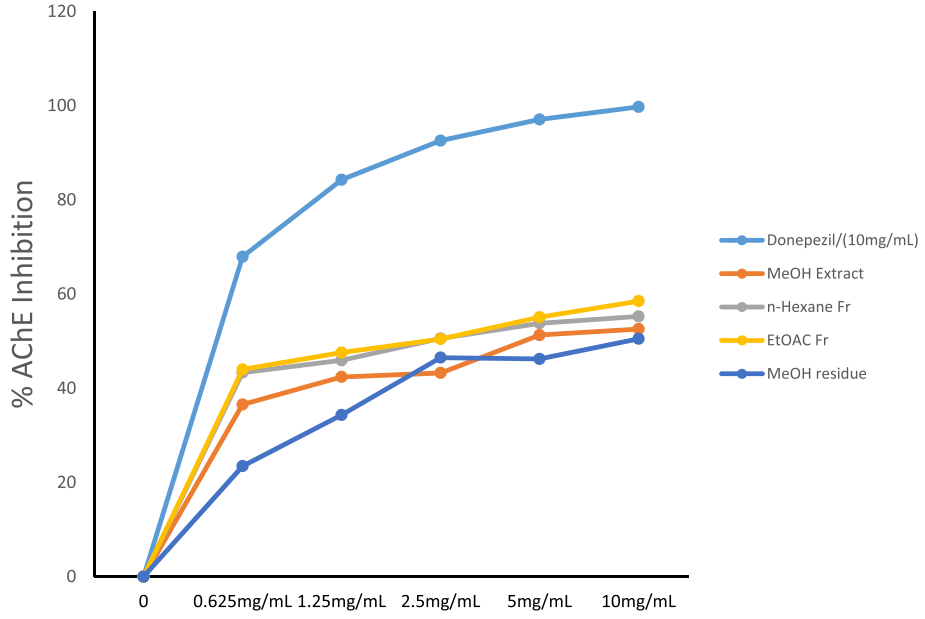


Fig. 1. AChE inhibitory activity of the methanol extract and solvent-solvent partition fractions of *O. gratissimum* leaves. Data are expressed as mean ± SD ($n = 2$). MeOH—methanol extract; EtOAc—ethylacetate fraction; Res MeOH—residual fraction after partitioning with n-hexane and ethylacetate.

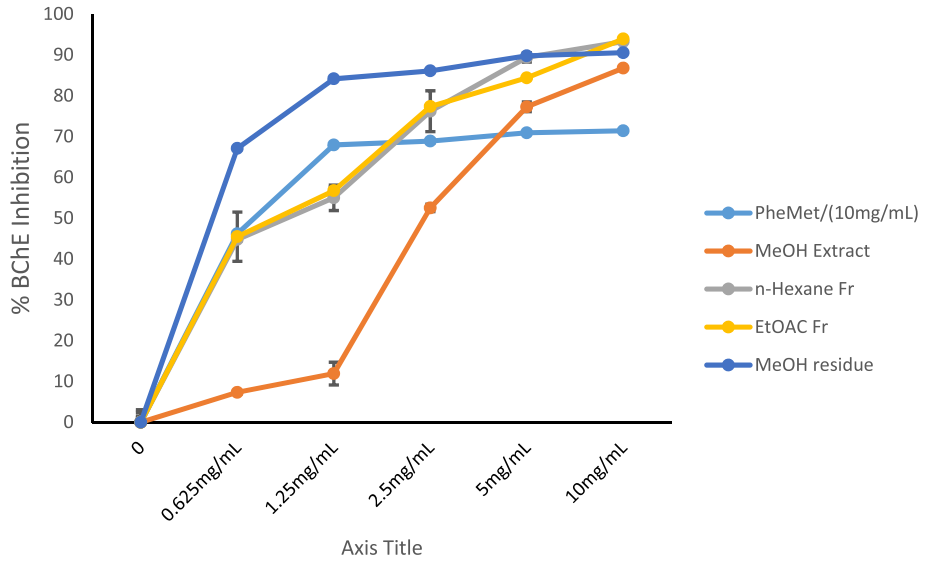


Fig. 2. BChE inhibitory activity of the methanol extract and solvent-solvent partition fractions of *O. gratissimum* leaves. Data are expressed as mean ± SD ($n = 2$). MeOH—methanol extract; EtOAc—ethylacetate fraction; Res MeOH—residual fraction after partitioning with n-hexane and ethylacetate.

inexperienced molecular docking analysis [22]. Targeting multiple etiological players of NDs has been a recent strategy for the development of potential therapeutics for NDs. Several medicinal plants and food herbs are known for their neuroprotective and antioxidant activities, as they have been traditionally used for the treatment of AD and other ND. These plants include: Crocus sativus [23], Nigella sativa [24], Coriandrum sativum [25], Ferula assafoetida [26], Thymus vulgaris [27], Zataria multiflora [28], Curcuma longa [26] and Gongronema latifolium [29]. Ocimum gratissimum, also known as "Scent leaf" or "Chit--Chan-Than" [30], is a perennial herb that belongs to the Lamiaceae family. *Ocimum gratissimum* is known for its aromatic flavor and is commonly used as a seasoning in traditional cuisines [30]. Despite documented evidence on the neuroprotective activities of different extracts of O. gratissimum [31,32], and inhibitory activities against cholinergic targets in different experimental models [33–35], neurotherapeutic components have not been documented. Therefore, the present study investigates the inhibitory potential of methanol extracts and solvent partition fraction of the extract on the cholinesterase and monoamine oxidase activities *in vitro*. Also, the GC-MS identified compounds from the selected fraction was screened against human acetylcholinesterase, butyrylcholinesterase and MAO-B enzymes using different computational approaches including molecular docking, ensemble-docking, molecular dynamics, clustering and ADMET filtering analysis.

Table 2
IC_{50} (mg/mL) of methanol extract, solvent partition fraction and reference inhibitors.

IC_{50} (mg/mL)	MeOH Extract	n-Hexane Frac	EtOAC Frac	MeOH Residue	Ref. inhibitors
AChE	2.380	2.022	2.066	1.079	0.1062
BChE	2.261	2.126	2.630	1.465	0.1452
MAO B	2.345	1.584	2.933	2.935	0.3223

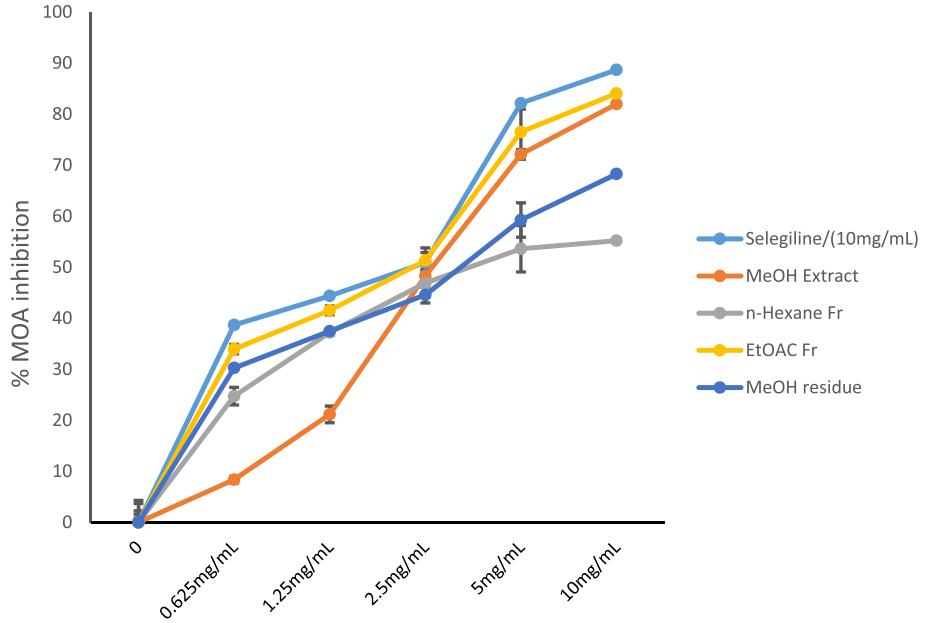


Fig. 3. Monoamine oxidase inhibitory activity of the methanol extract and solvent-solvent partition fractions of *O. gratissimum* leaves. Data are expressed as mean ± SD ($n = 2$). MeOH—methanol extract; EtOAc—ethylacetate fraction; Res MeOH—residual fraction after partitioning with n-hexane and ethylacetate.

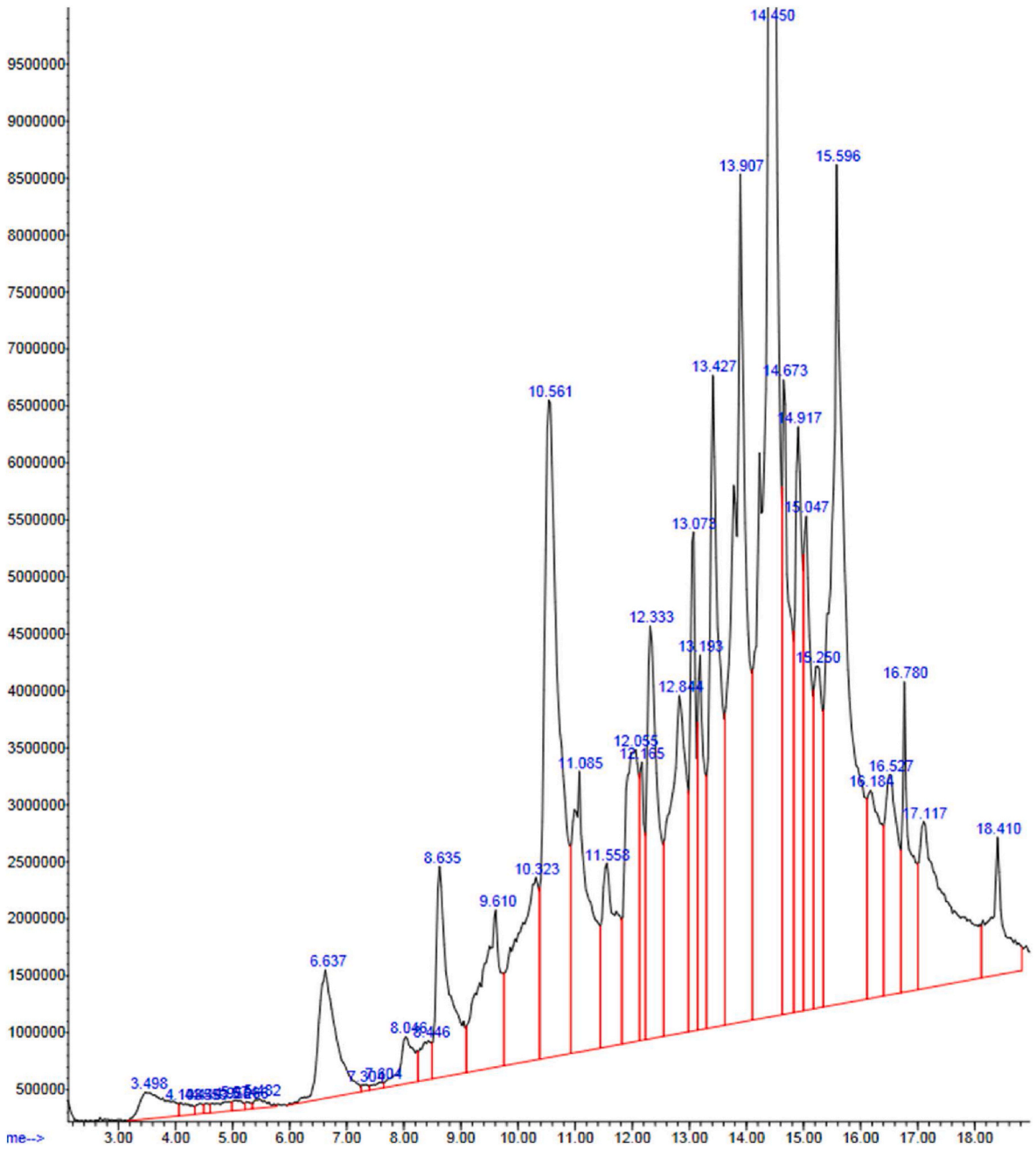


Fig. 4. Chromatogram of phytocompounds in n-hexane fraction of methanol *O. gratissimum*.

2. Materials and methods

2.1. Plant material

The fresh leaves of *O. gratissimum* was collected from the environs of the University of Ilorin campus in Tanke, Ilorin-South L.G.A Kwara State, Nigeria. Prior to the experiments, the collected plant material was identified and authenticated at the Department of Botanical Science, University of Ilorin.

2.2. Extraction, solvent portioning

The methods described by Harbone [36], was used for the extraction and solvent portioning of *O. gratissimum* leaves. About 10 kg of the leaves of *O. gratissimum* were air-dried under shade until a constant weight was attained. The dried leaves were pulverized into powder using industrial blender. About 2.2 kg of the leaves powder was further macerated in methanol for 72 h respectively. The residue obtained from filtration was further macerated in methanol for 72 h. The extraction process was repeated. The filtrates were evaporated under reduced pressure using a rotary evaporator to obtain methanol extracts of *Ocimum gratissimum* leaves (MEOG) (222 g). The MEOG was further successively partitioned with n-hexane (3 L) and ethyl acetate (EtOAc) (3 L) in this order, giving rise to 3 fractions: n-hexane (60 g), EtOAc (82 g), and methanol residue (88 g), the fractions was collected and concentrated using a rotary evaporator (below 40 °C).

2.3. In vitro analysis

2.3.1. Determination of acetylcholinesterase and butyrylcholinesterase inhibitory activities

The AChE and BChE inhibitory activities of the extracts and solvent

Table 3
Identified compounds n-hexane fraction of methanol extract of *O. gratissimum*.

Peak No	Name of phytocompound	RT (min)	Peak height	Corr Max %	Area %
1	1,3-Cyclopentanediol	3.498	230126	3.40	0.520
2	Oxirane	4.103	109956	0.68	0.104
3	9-Hexadecenoic acid	4.440	90372	0.34	0.052
4	4-Heptanone, 2,3:5,6-diepoxy-2,6-dimethyl	4.553	84475	0.24	0.037
5	Decanoic acid	4.956	80787	0.79	0.12
6	D-Glucopyranoside	5.074	84681	0.47	0.07
7	Tridecanoic acid	5.266	65086	0.20	0.03
8	1,2-Cyclopentanediol	5.482	77909	0.55	0.08
9	Dodecanal	6.637	1111186	10.87	1.66
10	Triethylenediamine	7.304	58730	0.21	0.03
11	2-Hydroxyethyl vinyl sulfide	7.604	51933	0.28	0.04
12	1,4-Dioxaspiro[2.4] heptan-5-one	8.046	405968	3.15	0.48
13	8-Nonenoic acid	8.446	339370	2.03	0.31
14	Decanal	8.635	2.95E+08	2.02	2.024
15	Cyclohexasiloxane	9.61	1369313	14.81	2.26
16	Morpholine	10.323	1585676	20.06	3.07
17	Thymol	10.561	1.1E+09	7.54	7.53
18	Cycloheptasiloxane	11.085	2366231	22.42	3.43
19	1,2–15,16-Diepoxyhexadecane	11.558	1603159	12.84	1.96
20	Cyclooctasiloxane	12.055	2544199	18.29	2.80
21	Cyclooctasiloxane	12.165	1.34E+08	0.92	0.921
22	Dodecanoic acid	12.333	3588476	21.94	3.35
23	2-Decen-1-ol	12.844	2925430	26.52	4.05
24	Cholestane	13.073	3.11E+08	2.14	2.137
25	1-Chloroeicosane	13.193	2.54E+08	1.75	1.746
26	Tetradecanoic acid	13.427	6.99E+08	4.80	4.798
27	Hexadecanoic acid	13.907	7231700	55.28	8.45
28	n-Hexadecanoic acid	14.45	15989386	100.00	15.29
29	3-Ethoxy-1,1,1,7,7,7-hexamethyl-3, 5,5tris(trimethylsiloxy) tetrasilo xane	14.673	5.08E+08	3.49	3.487
30	9-Octadecenoic acid	14.917	5064762	19.89	3.04%
31	Z-10-Tetradecen-1-ol acetate	15.047	3.77E+08	2.59	2.585
32	2- Chloropropionic acid	15.25	3007623	13.29	2.03%
33	Oleic Acid	15.596	7065027	69.52	10.63
34	Tetradecanal	16.184	1817484	13.06	2.00%
35	7-Hexadecenoic acid	16.527	1930275	13.42	2.05%
36	3-methoxy-morphanin	16.78	2.58E+08	1.77	1.768
37	Erucic acid	17.117	1458602	23.81	3.64
38	Hexasiloxane	18.41	2.06E+08	9.23	1.410

RT: retention time; Corr area: Corrected area.

fractions were determined spectrophotometrically using acetylcholine iodide and butrrylcholine iodide as substrates according to the Ellman method [37] as modified by perry et al. [38] using acetylcholine iodide and butrylcholine iodide as substrates. 500 μL of 0.1 M phosphate buffer (PH 8.0), 200 μL of AChE enzyme solution, 100 μL solution of 3.3 mM 5, 5-dithio-bis (2-nitrobenzoic) acid were added to micro plates containing of 0.65, 12.5, 2.5, 5, and 10 mg/mL of the extract and partition fraction and 0.065, 0.125, 0.25, 0.5, and 1 mg of the reference compounds made by serial dilution in 5% DMSO. The mixture was incubated for 20 min at 25 °C. After 20 min, 100 μL of 0.05 mM acetylthiocholine iodide was

Table 4
The binding energies obtained from the Docking analysis of the GC-MS identified compounds against *human* Acetylcholinesterase, *human* Butyrylcholinesterase, and *human* Mono amine oxidase.

S/No	Ligands	Binding energy (Kcal/mol)		
		AChE	BChE	MAO-B
S1	donepezil (E = 306.68)	**−12.2**	**−9.6**	**-**
S2	Decamethonium (E = 261.56)	**-**	**−6.5**	**-**
1	Cholestane E = 492.75	**−9.9**	**−9**	**−11**
2	3-methoxy-morphanin E = 254.84	**−9.3**	**−8.2**	**−10.1**
S3	Safinamideb			**−9.8**
9	tert-Hexadecanethiol E = 117.51	−7.4	−5.6	−9.8
3	hexadecylester E = 423.46	−9.2	−8	−9
5	2, 3-dihydroxypropylester E = 127.89	−7.6	−7.1	−7.9
6	Erucic acid E = 99.56	−7.5	−6.2	−7.7
11	1-Triacontanol E = 178.25	−7.3	−6.3	−7.5
21	9-Octadecenoic acid E = 69.17	−5.7	−5.7	−7.5
4	Cyclopentaneundecanoic acid E = 250.37	−8.2	−6.2	−7.4
7	Oleic Acid E = 81.73	−7.5	−6.6	−7.2
12	Z E−2 13-Octadecadien-1-ol E = 98.72	−7.3	−6.1	−7.2
13	Chloroeicosane E = 57.14	−7.2	−5.3	−7.2
10	Thymol E = 95.97	−7.4	−6.2	−6.7
8	Z-10-Tetradecen-1-ol acetate E = 109.01	−7.5	−6	−6.6
17	Pentadecanoic acid E = 53.40	−6.7	−6.1	−6.5
15	Tetradecanoic acid E = 51.08	−6.9	−5.7	−6.5
14	Tridecanoic acid E = 46.34	−7.1	−5.3	−6.5
18	4-Isopropylcyclohexylamine E = 88.82	−6.6	−5.7	−6.2
16	1, 16-Diepoxyhexadecane E = 2891.04	−6.9	−5.5	−6.2
20	D-Glucopyranoside E = 184.73	−5.9	−5.7	−5.8
19	Dodecanal E = 40.38	−6.3	−5.3	−5.7
22	Ribonic acid E = 107.96	−5.3	−4.9	−4.9
23	1, 4-Dioxaspiro[2.4]heptan-5-one (E = 1606.32	−5	−4.9	−4.7
24	1, 3-Cyclopentanediol E = 245.28	−4.7	−4.7	−4.5
25	1, 2-Cyclopentanediol E = 246.22	−4.7	−4.6	−4.2
26	Morpholine E = 88.94	−3.7	−3.6	−3.5
27	2-Hydroxyethyl vinyl sulfide E = 55.69	−3.6	−3.4	−3.5
28	Oxirane E = 1391.23	−2.3	−2.2	−2

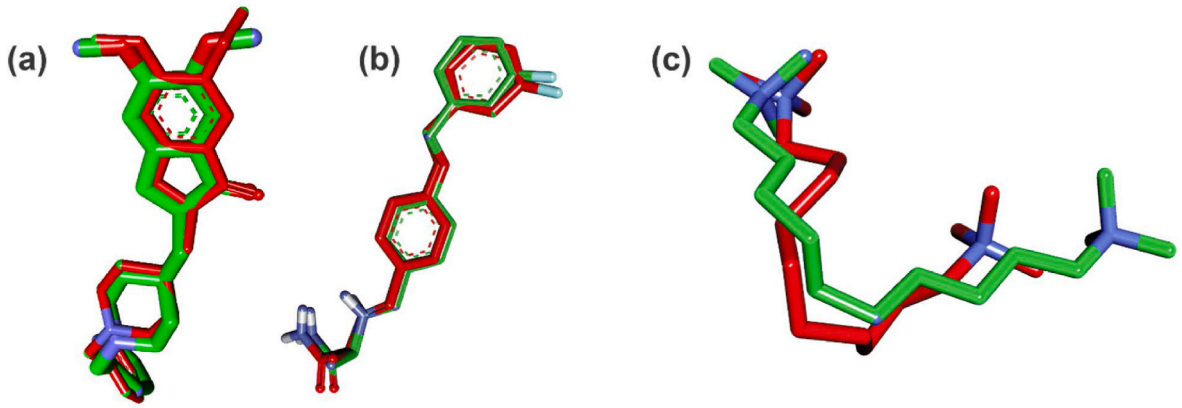


Fig. 5. Superimposition of docked conformer of the native ligand on the extracted conformation of (a) donepezil, (b) safinamide and (c) decamethonium. *Red: selected docked conformer and Green: extracted native ligand conformer.* (For interpretation of the references to colour in this figure legend, the reader is referred to the Web version of this article.)

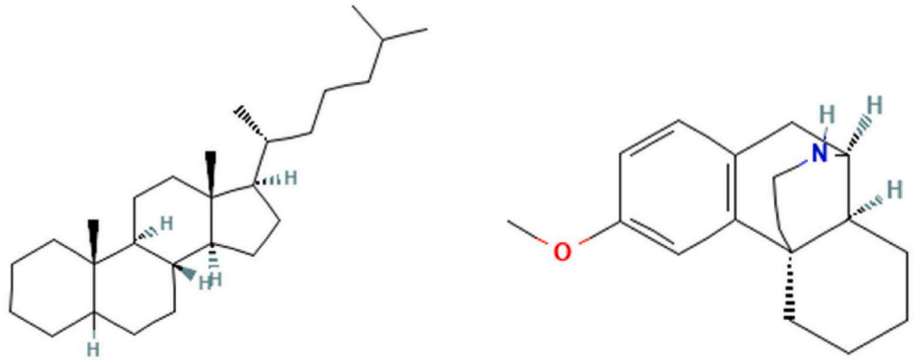


Fig. 6. Chemical structure of lead phytochemicals (a) Cholestane (b) 3-Methoxy-morphanin.

Table 5
Molecular interactions of the amino acid residues of AChE, BChE and MAO-B with the phytochemicals and reference inhibitors.

Compounds	Protein	Hydrogen bonds Bond distance (Å)			Hydrophobic Interaction
		Numbers	Interacted residues	Numbers	Interacted residues
Donepezil		1	Phe295	8	Phe338 Tyr337 His447 Tyr341(2) Trp86 Trp286 (2)
Cholestane	*h*AChE	0		15	Asn87 Trp86(2), Phe297 Trp286(3) Phe338 Tyr337(2) Tyr341(4) His447
3-methoxy-morphanin		1	Tyr124	5	Trp86 (2) His447
Decamethonium	***h***BChE	2	Tyr128 Pro285	5	Asp70 Tyr332 Tyr82 Glu197
Cholestane		0		7	Trp82(2) Ala328 Tyr332(3) Trp430 His438
3-methoxy-morphanin		8		4	Trp82(2) Ala328 Tyr332 Trp430
Safinamide	MAO B	3	Ile199 Gln206(2)	6	Ile199 Tyr326 Tyr398 Leu171Cys172 Ile316
Cholestane		0		14	Tyr326 (2) Ile199 Met436 Tyr435(3) Tyr398(4) Leu171(2) Cys172
3-methoxy-morphanin		2	Met436 Gly58	5	Tyr435 Tyr398 Gly57

added to the mixture and the AChE activity that occurred within 3 min at room temperature was measured at 412 nm.

Using butyrylthiocholine as substrate, the same protocol was adopted to measure BChE activity [38]. The inhibitory activity of the enzyme was computed and presented as percentage inhibition. 5% DMSO was used as the negative control while the assay was carried out in duplicates

$$\text{Inhibition } \% = [(Abs_{cont}\text{-}Ab_{sam})/Abs_{cont}] \text{ x } 100 \quad \text{Equation 1}$$

where Abs_{cont} is the change in absorbance of the negative control, and Ab_{sam} is the change in absorbance of the sample.

2.3.2. Determination of monoamine oxidase inhibitory activities

The monoamine Oxidase Inhibitory activities of the extracts and partition fractions were determined based on slight modification of previously reported method [39]. The reaction mixture comprised phosphate buffer (0.025 M at pH7), semicarbazide (12.5 mM), benzylamine (10 mM at pH 7), 75 μL of enzyme (MAO B) and 0.65, 12.5, 2.5, 5, and 10 mg/mL of the extract and partition fraction and 0.065, 0.125, 0.25, 0.5, and 1 mg of the reference compound (selegiline) made by serial dilution in 5% DMSO. Acetic acid (250 μL) was added after 30 min, and boiled for 3 min in water bath, thereafter, the mixture was centrifuged. The resultant supernatant (1 mL), 0.05% 2, 4-DNPH (1.25 mL), and 1.25 mL benzene were mixed prior to the incubation at room temperature for 10 min. Equal volumes of sodium hydroxide (1 N) and separated benzene layer of the mixture above were mixed together and heated for 10 min at 80 °C. The alkaline layer was decanted and the absorbance was measured in duplicates at 450 nm. The inhibition in percentage was calculated as follows:

$$\text{Inhibition } \% = [(Abs_{Control} - Abs_{Samples})/Abs_{Control}] \times 100 \quad \text{Equation 2}$$

2.4. Statistical analysis

Microsoft Excel, 2021, GraphPad Prism 8.0 was used for data analysis. One-way analysis of variance (ANOVA) with Duncan Multiple Range post hoc analysis was used to find the statistical differences among the means. The data were expressed as the mean ± SEM and $p < 0.05$ were considered as significant differences.

2.5. Gas chromatography-mass spectrometer (GC-MS) analysis

A gas chromatography from Agilent USA hypherated to a mass spectrophotometer (5975C) with triple axis detector equipped with an auto injector (10ul syringe) was used, Helium gas was used as a carrier gas.

The chromatographic investigations was executed on capillary column that was treated with phenyl methyl silox, with thickness (250 μm) internal diameter (0.2 μm), length (30 m). The other conditions for GC-MS were interface temperature (300^{O}C), ion source temperature (EI) (250^{O}C), pressure: 16.2 psia, out time (1.8 mm), 1 μL injector in Split mode with split ratio 1:50 with the temperature for injection at 280^{O}C and a changed of column temperature at the rate of 20 ^{O}C/minutes from the initial 50 ^{O}C to 100 ^{O}C for the first 2 min and a raised to 250^{O}C and held for 5 min. The total elution was 19mins. The relative percentage of the phytochemicals in the extract was expressed as the percentage with peak area normalization as previously reported by Lawal et al. [40]. The relative percentage amount of each phytocompound was computed by comparing its average peak area to the total area. The database of National Institute Standard and Technology (NIST) with more than 62 000 patterns was used for mass spectrum interpretation.

2.6. In silico studies

2.6.1. Molecular docking analysis

2.6.1.1. Ligand preparation. Donepezil, decamethonium, safinamide and 38 compounds that were identified from the GC-MS analsysis of the n-hexane partition fraction of *O. gratissimum* were retrieved from http://www.pubchem.ncbi.nlm.nih.gov, PubChem database, in structure data

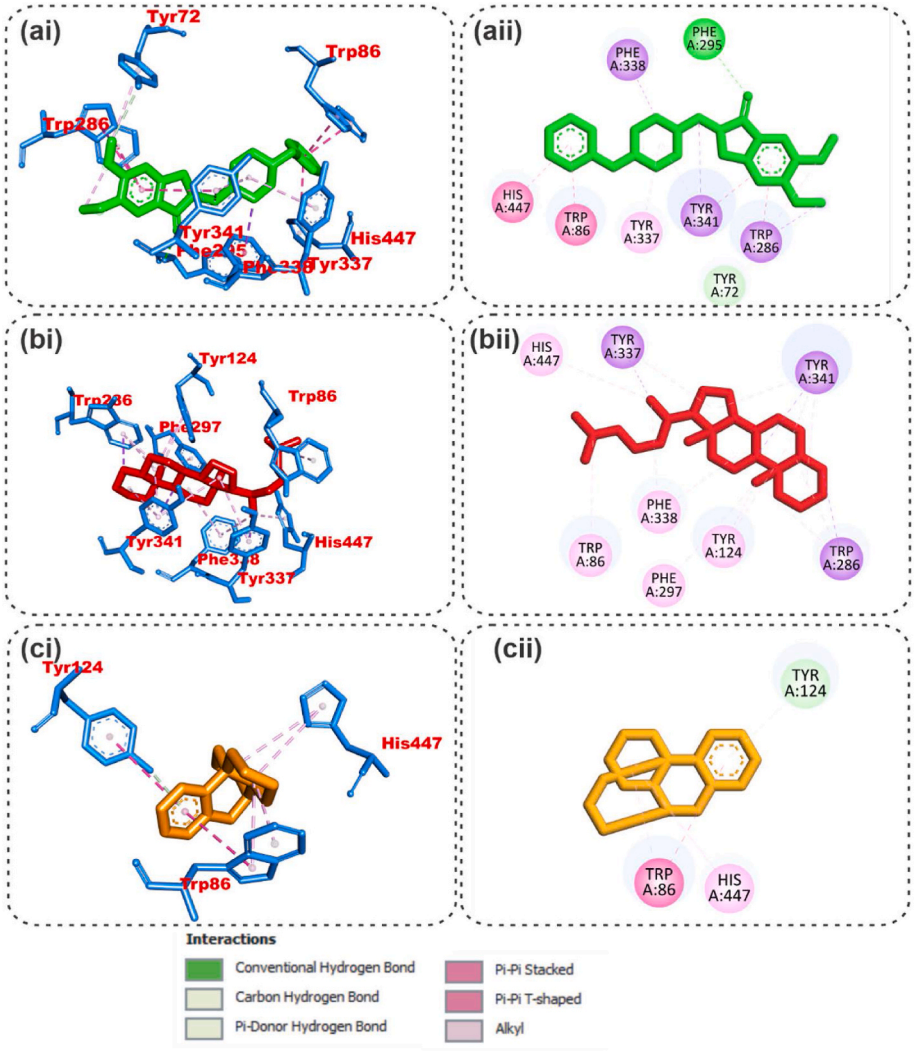


Fig. 7. Amino acid interactions of lead phytochemicals and reference inhibitor from the docking analysis of GC-MS identified compounds from *Ocimum gratissimum* in the active site groove of *human* butyrylcholinesterase. The ligands are presented in stick representations and differentiated by colours **(a)** Green: donepezil (reference inhibitor) **(b)** Red: cholestane **(c)** gold: 3-methoxy-morphanin. (For interpretation of the references to colour in this figure legend, the reader is referred to the Web version of this article.)

file (SDF) format, and converted to PDB (Protein Data Bank) format in Discovery Studio Visualizer, BIOVIA, 2020. The nonpolar hydrogens were merged with the carbons wile polar hydrogen charges of the Gasteiger-type were added and the internal degrees of freedom and torsions were determined. The proteins and ligands were then converted to PDBQT format using Autodock tools.

2.6.1.2. Protein preparation. The deposited co-crystallized structures of AChE with PDB ID: 4EY7 [41], BChE with PDB ID: 6EP4 [42] and MAO-B with PDB ID: 2V5Z [43] were downloaded from the PDB (http://www.rcsb.org). The proteins structures were prepared by removing water molecules and bound ligands, while hydrogen atoms were added using the add hydrogen atom in Autodock v4.2 program, Scripps Research Institute. Afterwards, the non-polar hydrogens were merged. The proteins were then saved as PDB and converted to PDB Partial Charge, & Atom Type (PDBQT) format in Autodock Vina [44] incorporated into PyRx 0.8 with the command "convert to macromolecule".

2.6.1.3. Validation of molecular docking protocol. The poses obtained from the docking of the co-crystalized ligands used as reference compounds in the study (donepezil, decamethonium and safinamide) having the lowest binding energy were aligned with the native ligands that were extracted from the downloaded structure in order to validate the protocol to be used for the virtual screening. The RMSD was computed in Discovery Studio Visualizer, BIOVIA, 2020.

2.6.1.4. Active site targeted molecular docking. Molecular docking simulation of ligands to respective protein receptors was performed using autodock Vina [44] incorporated into PyRx 0.8. The proteins in PDB format were imported into PyRx 0.8 and converted to PDBQT, while the ligands were imported into the Openbabel [45] section of the software. The ligands were subjected to minimization using conjugate gradient descent as the optimization algorithm and Universal Force Field (UFF) as the energy minimization parameter. For each of the proteins, the active site region as defined by the grid boxes with parameters defined in Table 1. The regions were mapped by selecting the amino acid that makes up the active site including residues that interacts with the co-crystallized ligands. The binding energies of reference compounds and phytocompounds for the three targets were recorded and then graded based on their affinity scores. Molecular interaction between the hit compounds were viewed with Discovery Studio Visualizer, BIOVIA, 2020.

2.6.2. Molecular dynamics

In this study, 2 different molecular dynamics studies were undertaken. The trajectories obtained from the first MDs analysis was used for cluster analysis. The unbound enzymes of the three enzymes were subjected to a 100 ns molecular dynamics simulation. The trajectories obtained from these MDs were used for conformational analysis using the

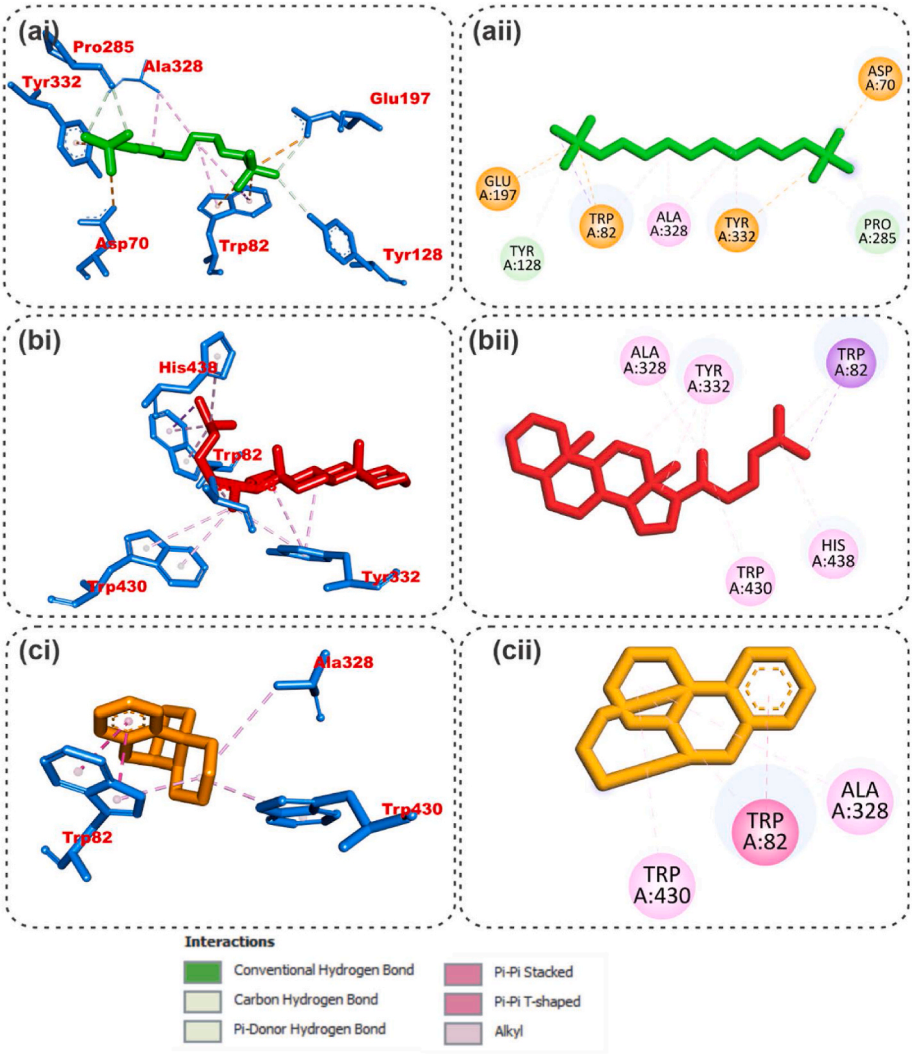


Fig. 8. Amino acid interactions of lead phytochemicals and reference inhibitor from the docking analysis of GC-MS identified compounds from Ocimum *gratissimum* in the active site groove of *human* butyrylcholinesterase. The ligands are presented in stick representations and differentiated by colours **(a)** Green: decamethonium (reference inhibitor) **(b)** Red: cholestane (**c**) gold: 3-methoxy-morphanin. (For interpretation of the references to colour in this figure legend, the reader is referred to the Web version of this article.)

TTclust. The second MDs analysis was performed to study the stability of the docked phytochemicals to the target enzymes. After the docking analysis, the unbound enzymes (2V5V, 4EY7 and 6EP4), and the enzyme complexed to the lead phytochemicals were subjected to full atomistic Molecular Dynamic (MD) simulation using GROMACS 2019.2 and GROMOS96 43a1 forcefield on the WebGRO server [46–48]. The topology files of the ligands were generated on PRODRG webserver (http://davapc1.bioch.dundee.ac.uk/cgi-bin/prodrg). The systems of the unbound enzymes and the ligand–bound enzymes complex was all solvated with transferable intermolecular potential with a four-point (TIP4P) within a cubic box water model, with periodic boundary conditions applied at a physiological concentration of 0.154 M set by neutralized NaCl ions. The systems were minimized for 10000 steps using steepest descent algorithm in constant number of atoms, volume, and temperature ensemble (NVT) ensemble for 0.3 ns, followed by 0.3 ns of equilibration in constant number of atoms, constant pressure and constant temperature (NPT). Temperature and pressure were set to 310 K and 1 atm respectively and maintained using velocity rescale and Parrinello-Rahmanbarostat, respectively. Leap-frog integrator was used with a time step of 2 fs. For each system, 50 ns of simulation was performed and for each 0.1 nano a snapshot was saved with a total of 1000 frame from each system. The VMD TK console scripts [49] was used to analyse the trajectories generated from the simulation to calculate RMSD, RMSF, SASA, RoG, and number of H-bond.

2.6.3. *Clustering of molecular dynamic trajectories of unbound proteins*

In this study, 2 different approach of clustering was used for the clustering analysis. The first was the clustering of the 100 ns MD trajectories of the unbound enzymes. A representative conformer of each cluster will be used for ensemble-docking analysis. The second cluster analysis will be undertaken on the 50 ns MD trajectories of the complexes of the lead phytochemicals that was obtained after docking analysis. The purpose of this clustering analysis is to investigated the stability of the ligand bound enzyme during the period of the simulation. TTClust V 4.9.0 [50] was used to cluster the trajectories from the MD simulation. The systems were clustered automatically utilizing TTClust python package, that utilizes the elbow method to determine the optimal number of clusters, and finally producing a representative frame for each cluster. A representative conformation from each cluster was will be selected. The analysis of each cluster was based on RMSD values, with reference to the starting geometry and the minimum energy conformation of the most populated cluster was taken as the most reliable solution.

2.6.4. *Ensembled-based docking of the GC-MS identified phytochemicals to different conformation from molecular dynamics trajectories*

The first five lead phytocompounds and the reference compounds were docked to the different representative conformers of 4EY7 (4), 6EP4 (4) and 2V5V (6) that were obtained from the cluster analysis of the trajectories obtained from the MD simulation using AutoDock Vina

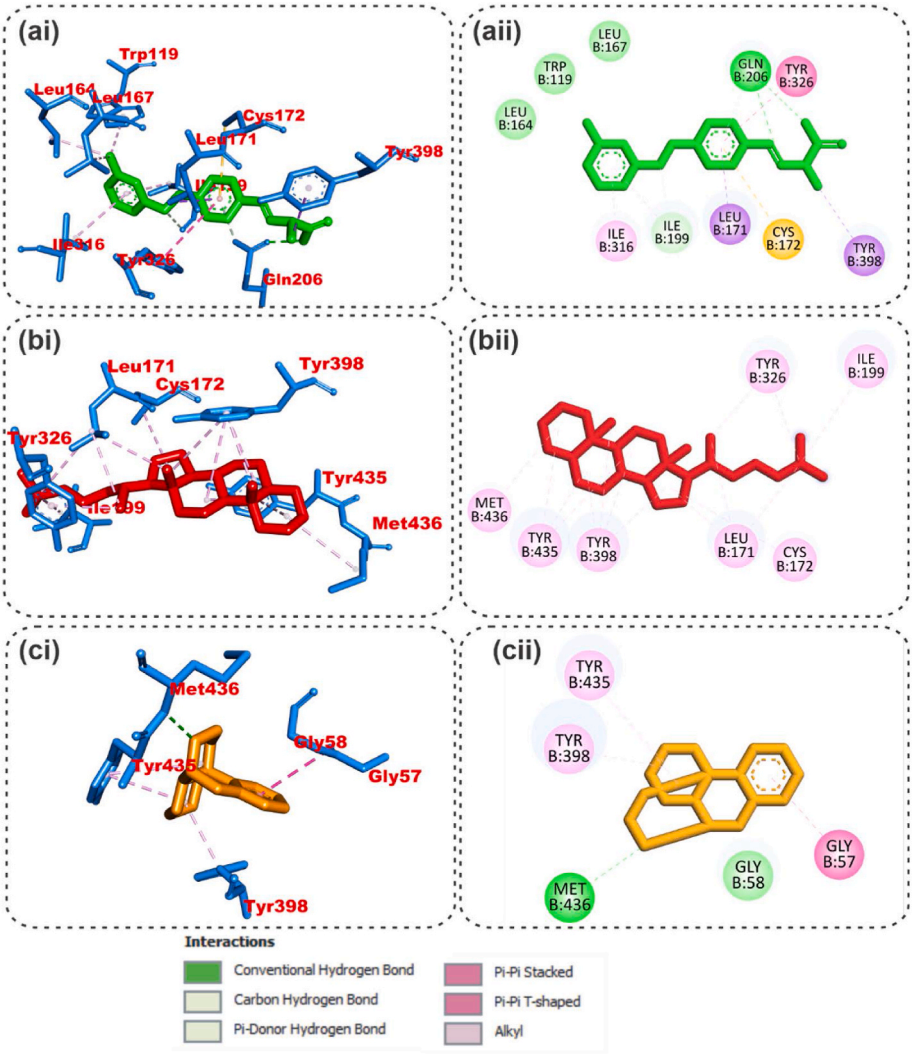


Fig. 9. Amino acid interactions of lead phytochemicals and reference inhibitor from the docking analysis of GC-MS identified compounds from Ocimum *gratissimum* in the active site of *human* mono amine oxidase. The ligands are presented in stick representations and differentiated by colours **(a)** Green: Safinamide (reference inhibitor) **(b)** Red: Cholestane (**c**) gold: 3-methoxy-morphanin. (For interpretation of the references to colour in this figure legend, the reader is referred to the Web version of this article.)

software [44]. After docking of the compounds to the representative conformation of each of the clusters, the average binding energy to each protein was calculated by finding the average binding energies of each ligand to the different cluster of the protein [51,52]. The average binding energy of compounds for the two targets were recorded and then graded by their affinity scores. Molecular interactions between the lead compounds were viewed with Discovery Studio Visualizer, BIOVIA, 2020.

2.6.5. *In silico physicochemical properties and ADMET analysis of lead phytochemicals*

The two lead phytochemicals were subjected to drug-likeness and ADMET filtering analysis over a wide range of descriptors. The drug-likeness analysis using the Verber and Lipinski filtering tools, was executed on the SwissADME webserver (http://www.swissadme.ch/index.php), while the predicted Absorption, Distribution, Metabolism, Excretion and toxicity (ADME/tox) analysis was performed on the SuperPred webserver (http://lmmd.ecust.edu.cn/admetsar1/predict/). The canonical SMILES of the lead phytocompounds were obtained from PubChem Database or copied from ChemDraw to calculate ADMET properties using default parameters.

3. Results

3.1. *In vitro studies*

3.1.1. *Cholinesterase and monoamine oxidase inhibitory activities*

The inhibitory effect of MEOG, solvent partition fraction and reference inhibitors on cholinesterase (AChE and BChE) and monoamine oxidase (MAO B) activities (*in vitro*) was investigated using donepezil, phenazine methosulfate and selegiline as reference inhibitors respectively. From the percentage inhibitory activities of the extracts and solvent fractions against AChE, BChE and MAO-B there was a concentration-dependent inhibition of the enzymes (Figs. 1–3). The respective IC_{50} of the inhibitory effect of the methanol extract, n-hexane, ethylacetate solvent fraction and the residue methanol fraction is presented Table 2. It was observed for AChE inhibitory activity, the three partition fractions (n-hexane, ethylacetate and residual methanol) had lower IC_{50} than the crude extract, this trend was also observed for the percentage inhibition. In the same manner the solvent fractions presented lower IC_{50} when compared to the methanol extract for BChE inhibitory activities. For MAO-B inhibitory activity, the IC_{50} of the methanol extract was lower compared to the solvent fractions. While the n-haxane fraction had the lowest IC_{50}. The result further suggests a better inhibition of AChE when compared to BChE based on the IC_{50}, although the methanol extract and the solvent fractions had better percentage inhibition for BChE (Table 2). The n-hexane was selected for

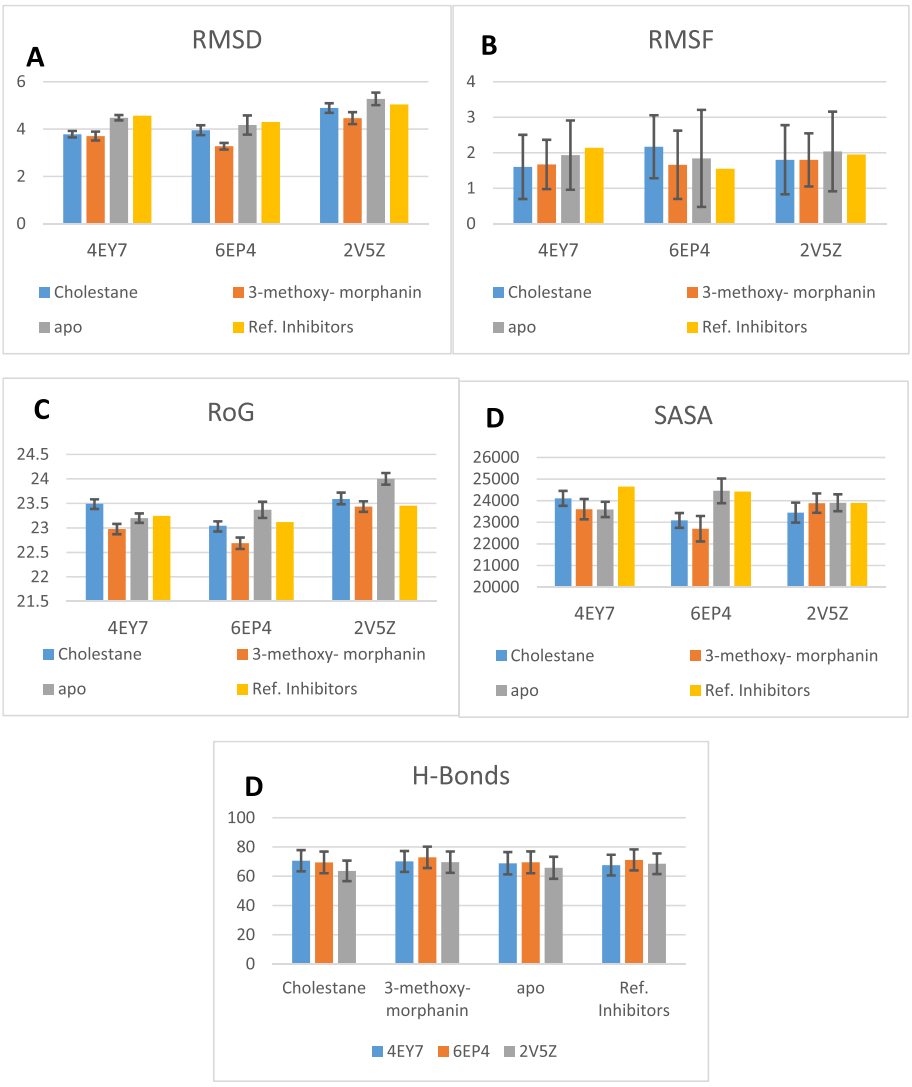


Fig. 10. Means and standard deviation of various parameters computed from the trajectories of molecular dynamic simulation. (A) Root Mean Square Deviation (RMSD) (B) Root Mean Square Fluctuations (RMSF) (C) Radius of gyration (RoG) (D) Surface Accessible Surface Area (SASA) (E) H-bonds during the MDS trajectory.

GC-MS analysis based on the percentage inhibition and IC_{50}.

3.2. GC-MS identification of chemical constituent

The GC-MS chromatogram of the n-hexane fraction of methanol extract of *O. gratissimum* leaves (Fig. 4), show the peaks of the compounds identified in the fraction. The phytocompounds were identified based on retention time and the peak area. Table 3 shows the name of the phytocompounds, retention time (RT), the peak height and percentage peak area. A total of 38 compounds were identified. n-hexadecanoic acid, hexadecanoic acid and Thymol with close RT of 14.450, 13.907 and 10.561 were identified to have the highest percentage area, signifying the abundance of the compound in the fraction. Cholestane has a peak number 24, RT 13.073 and % area 2.137, morphanin has a peak number 36, RT 16.78 and % area 1.72 (Fig. 4).

3.3. Results of in silico analysis

3.3.1. Validation of molecular docking protocol

The validation of the protocol used for the docking analysis, shows that the superimposition of conformation with the least binding energy from the docking analysis of the co-crystallized ligands on the extracted native ligands produced a very low RMSD of 0.5761, 0.4985 and 2.2025 Å for donepezil, decamethonium and safinamide respectively. The RMSD values were computed using BIOVIA Discovery Studio Visualizer 20.1.0, San Diego, CA, USA 2020) (Fig. 5).

3.3.2. Binding affinity and interaction of lead phytochemicals to target enzymes

Thirty-six (36) compounds identified by the GC-MS analysis, were considered in this study.

The binding energy from the docking analysis is presented in Table 4. Except for donepezil the reference standard for AChE, the two phytocompounds (Cholestane and 3-methoxy-morphanin) Fig. 6 with highest binding energies were comparable and higher when compared to the reference compounds for BChE and MAO B respectively. It was observed that the lead phytochemicals from the docking analysis presented multiple binding tendencies to the three enzymes that were studied. It was also observed that Cholestane had the highest binding energy of −9.9, −9.0 and −11 kcal/mol for AChE, BChE and MAO B Kcal/mol respectively, while 3-methoxy-morphanin presented a binding energy of −9.3, −8.2 and −10.1 kcal/mol respectively. Notably the cholestane and 3-methoxy-morphanin two lead phytochemicals presented higher binding energies (−11 and −10.1 kcal/mol) when compared to safinamideb (−9.8 kcal/mol) the reference inhibitor of MAO B. Beside the two lead compounds that were selected based on their highest binding energies, orientation in the catalytic sites of the enzymes and interaction with catalytic residues, hexadecylester and Cyclopentaneundecanoic acid

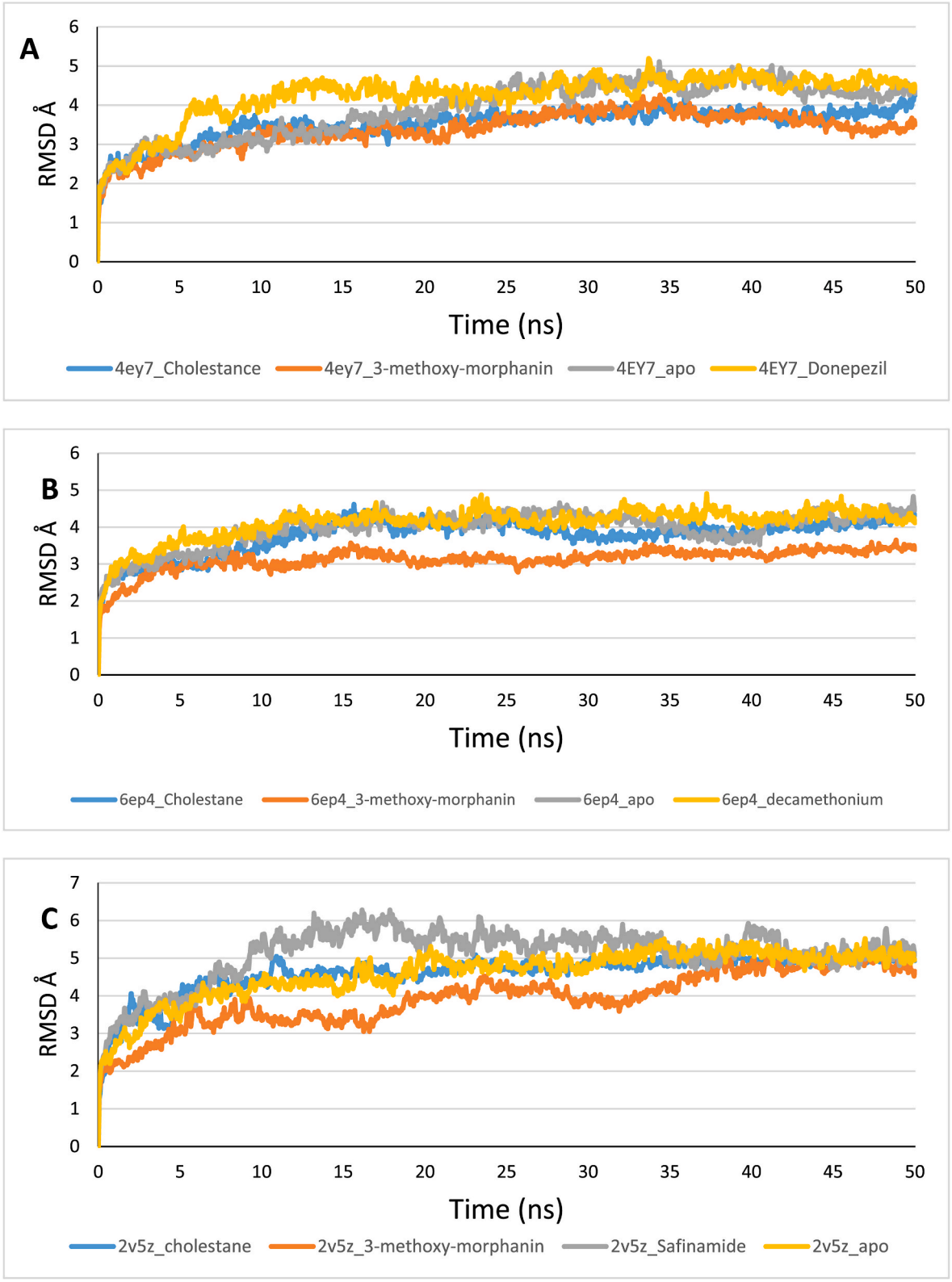


Fig. 11. The Backbone-RMSD plots of molecular dynamics (MD) simulation of unbound and enzyme-ligand complexed to (a) *human* acetylcholinesterase (*h*AChE) (b) *human* butyrylcholinesterase (*h*BChE) (c) *human* Monoamine oxidase (MAO-B).

and 2, 3-dihydroxypropylester the 3rd, 4th 5th hit phytochemical from the docking analysis to AChE. Hexadecylester, 2, 3-dihydroxypropylester and oleic acid were the 3rd, 4th 5th hit phytochemical against BChE while tert-Hexadecanethiol, hexadecylester, 2, 3-dihydroxypropylester the 3rd 4th 5th hit phytochemical to MAO-B.

3.3.3. Amino acid interactions of selected phytochemicals with the active site of human AChE, BChE, and MAO-B

The lead phytochemicals (cholestane and 3-methoxy-morphanin) (Fig. 6) and reference compounds were selected for interactive analysis. Table 5 shows the various binding interactions in the active groove

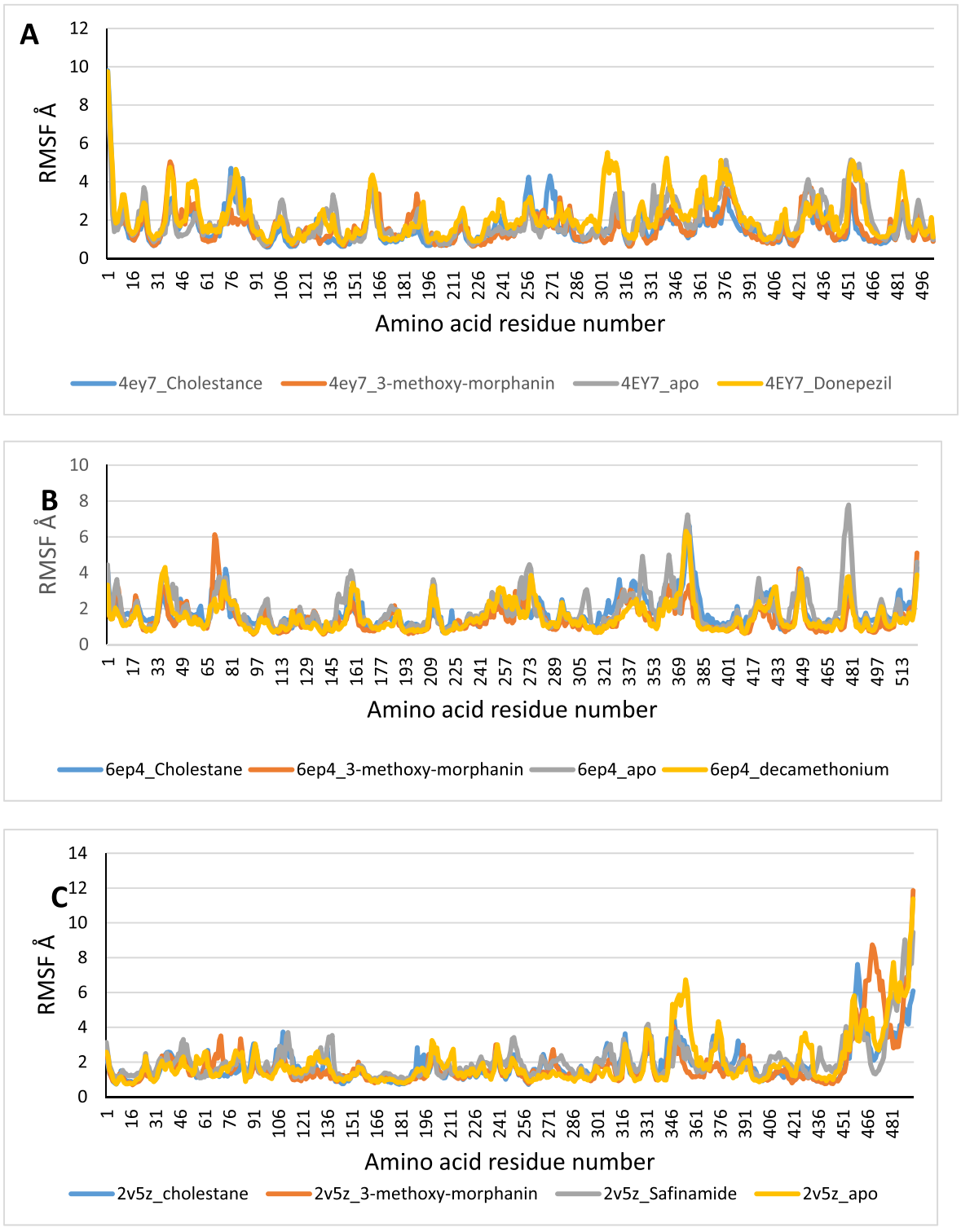


Fig. 12. Per residue RMSF plots of molecular dynamics (MD) simulation of unbound and enzyme-ligand complexes to (a) human acetylcholinesterase (*h*AChE) (b) *human* butyrylcholinesterase (*h*BChE) (c) *human* Monoamine oxidase (MAO-B).

of the proteins. The interactions between the ligand groups of donepezil (co-crystalized ligand) with human AChE (*h*AChE) showed that donepezil was docked into the active site gorge. The revalidated docked donepezil was similarly stretched in the gorge as the co-crystalized ligand. The 1-benzyl unit of donepezil interacted in an aromatic Pi-Pi stacking to Trp86 and His447. The piperidine ring formed 2 Pi-Alkyl contacts with Tyr337 and Tyr341 of *h*AChE. 2 Pi-sigma bonds were observed between the 5-methoxy unit of inden-1-one, the piperidine ring, and Trp286 and Phe338 respectively. Only a hydrogen bond was formed between the carbonyl oxygen of the indenone ring and Phe295 (Fig. 7). The rings of cholestane made 3 Pi-sigma interactions with Tyr337, Tyr341 and Trp286, while it interacted with the remaining amino acid through Pi-alkyl interaction to form a hydrogen bond with Tyr124 while a Pi-Pi-stacking and Pi-alkyl interaction was observed with Trp86 and His447 respectively (Fig. 7).

In the case of *h*BChE, decamethonium was docked deep into the

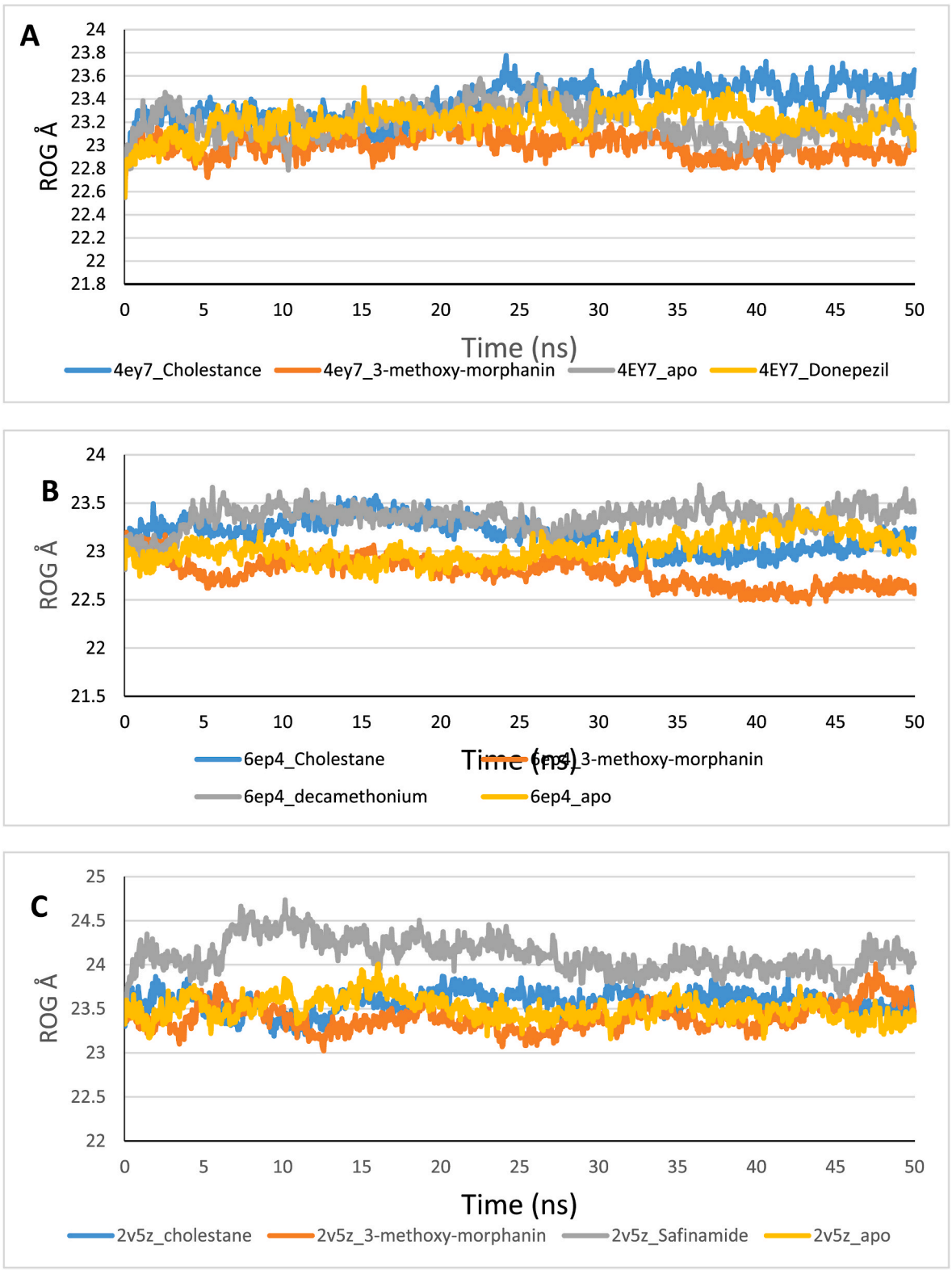


Fig. 13. The RoG plots of molecular dynamics (MD) simulation of unbound and enzyme-ligand complexes (a) *human* acetylcholinesterase (*h*AChE) (b) *human* butyrylcholinesterase (*h*BChE) (c) *human* Monoamine oxidase (MAO-B).

active site gorge aligning in the same pattern as the native ligand. This is evident from the overlap of the docked conform, when it was superimposed on the native ligand. Attractive charge and Pi-cation interactions were made with Glu197, Trp82 Tyr332 and Asp70, while Pi-Sigma contact was made with Trp82. Cholestane also formed as Pi-Sigma contact with Trp82, while the rings interacted via Pi-alkyl and alkyl interaction with Ala328, Tyr332 Tyr332 of the P-site, Trp430 and His438. also interacted with Trp82 via Pi-Pi-stacking while Pi-alkyl and alkyl contacts were made to Ala382 and Trp430 (Fig. 8). The conformer of safinamide, the reference inhibitor of MAO-B was orientated in the

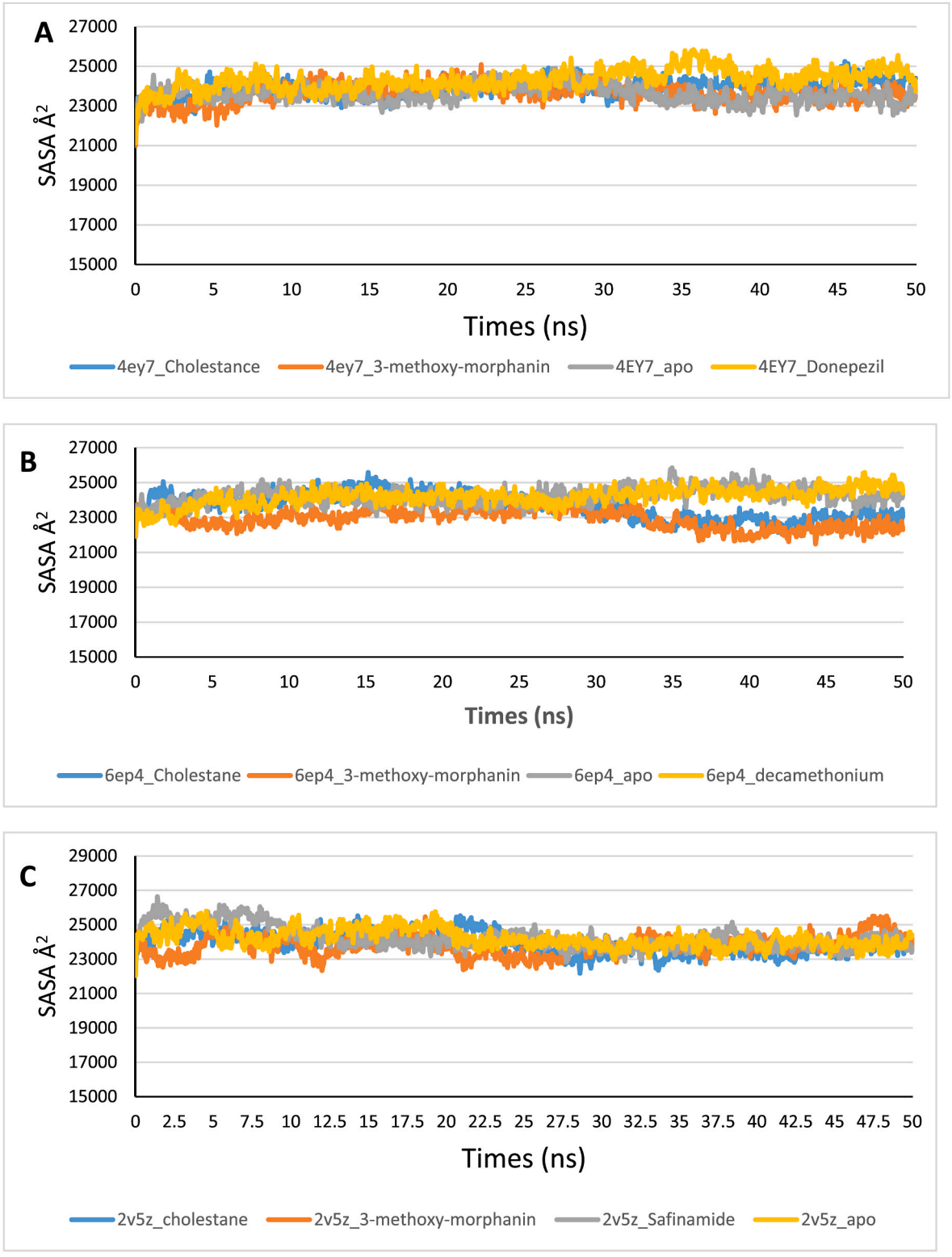


Fig. 14. The SASA plots of molecular dynamics (MD) simulation of unbound and enzyme-ligand complexes (a) *human* acetylcholinesterase (hAChE) (b) *human* butyrylcholinesterase (hBChE) (c) *human* Monoamine oxidase (MAO-B).

active site of the enzyme in similar binding pattern as the co-crystalized ligand. The lead phytochemicals were orientated into the active site of MAO B B in a similar binding pattern as the reference compounds safinamide. the lead phytocompounds interacted with Tyr60, Tyr326, and Gln206 that lines the niche of the substrate cavity and Tyr326 that lies at the top of the cavity (Fig. 9).

3.3.4. Molecular dynamics

The stability of the enzymes complexed with the lead phytochemicals (cholestane and 3-methoxy-morphanin) and respective reference inhibitors as compared with the apo (unbound) enzymes was observed during the period of molecular using the Tk console scripts in VMD version 1.9.3. The trajectories obtained from the simulation was

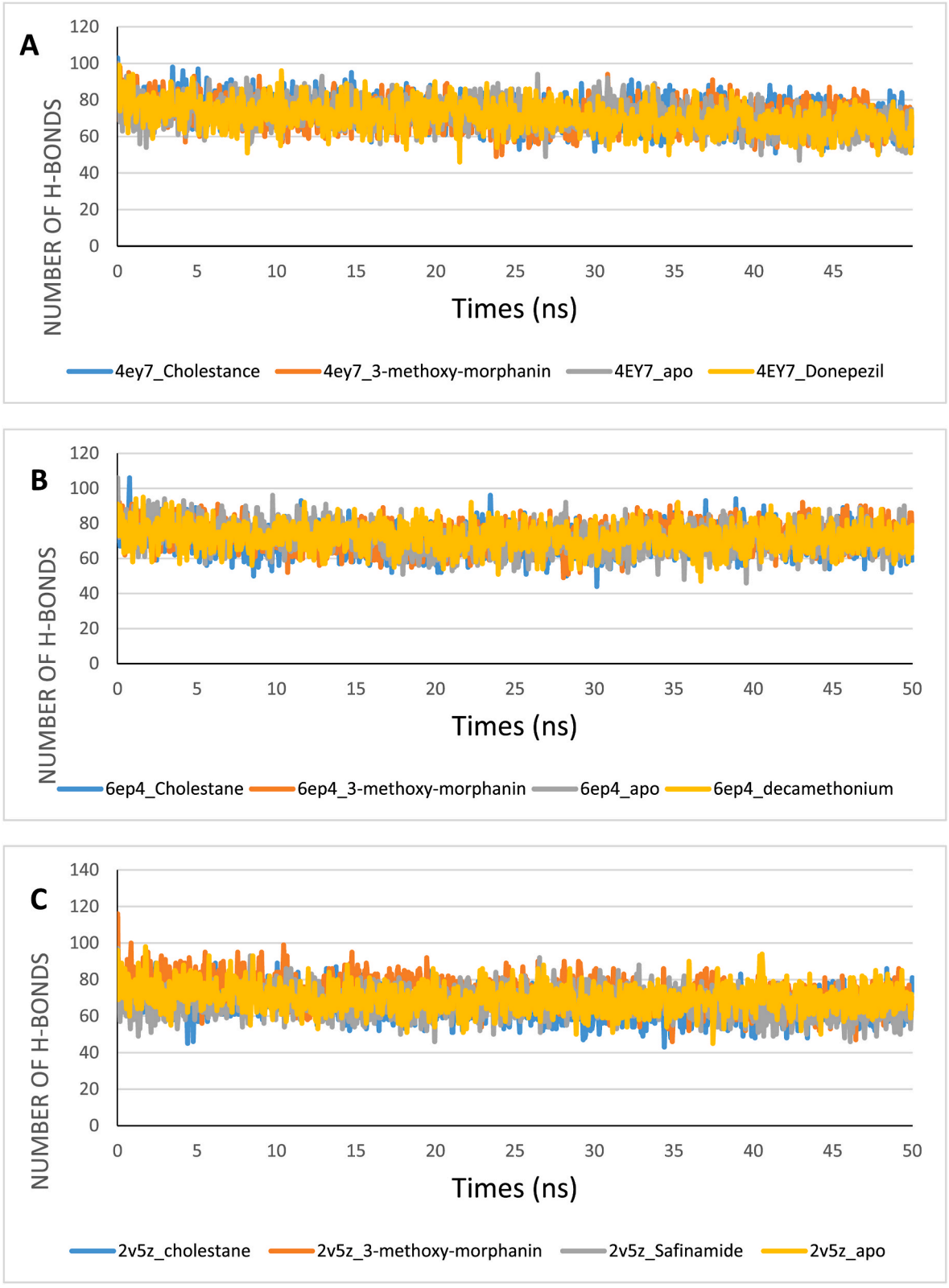


Fig. 15. The changes in the number of H-bonds during the MDS trajectory of unbound and enzyme-ligand complexes (a) *human* acetylcholinesterase (hAChE) (b) *human* butyrylcholinesterase (hBChE) (c) *human* Monoamine oxidase (MAO-B).

analysed using the RMSD, RMSF, RoG, SASA and number of H-bonds. The means and standard deviations of the parameters studied are presented in Fig. 10. The spectra plot for bond and unbound enzymes are presented in Figs. 11–15. The RMSD plots reveals the degree of deviation of each frame from the initial structure, hence it is used to measure the stability of the protein structure during the period of the simulation. For the RMSD plots for *h*AChE, *h*BChE and MAO-B, the systems were equilibrated around 10 ns with minimal fluctuation that was less than 3

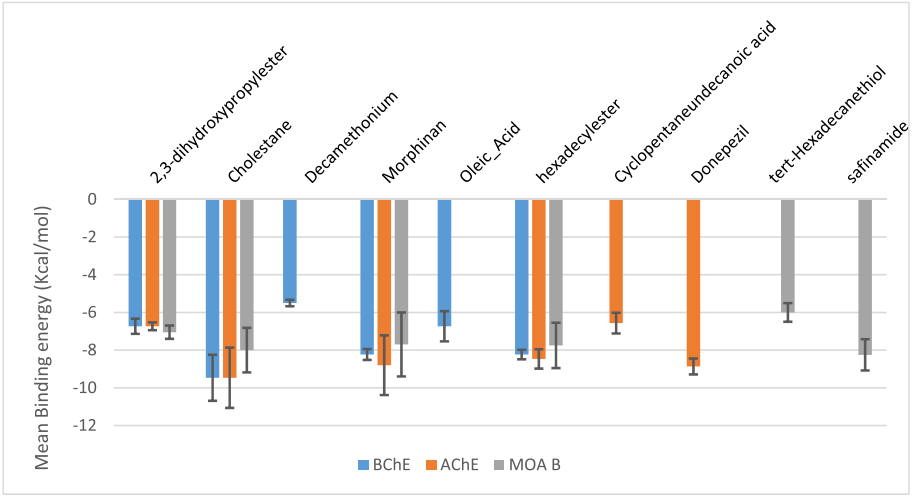


Fig. 16. The average binding energies of the reference inhibitors and five lead phytochemicals against representative conformation gotten from the clustering analysis of the MD simulation trajectories of AChE, BChE and MAO-B enzyme. Number of clusters: AChE (4), BChE (4) and MAO-B (6) enzyme.

Table 6
The interactions of the two lead phytochemicals and reference inhibitors with the best representative conformation from the cluster analysis of human AChE, BChE and MAO-B molecular dynamics simulation trajectories.

Compounds	Protein	Hydrogen bonds Bond distance (Å)			Hydrophobic Interaction
		Numbers	Interacted residues	Numbers	Interacted residues
Donepezil		2	GLy120 Tyr133	7	Gly121 Ile445 Gly442 Trp86 Leu130 Ala127 Val132
Cholestane	*h*AChE	0		4	Trp86, Ala127, Val132 Val73
3-methoxy-morphanin	Cluster 1	1	Glu	3	Gln71 Leu76 Met85
Decamethonium	***h***BChE	0	His438	4	Glu433 Phe76 Glu197 Glu441
Cholestane	Cluster 1	0		5	Trp82 Phe76 Pro429 Trp430 His438
3-methoxy-morphanin		0		4	Phe76 Pro429 Trp439 Ala328
Safinamide	MAO B	3	Gly58 Tyr60 Tyr398	6	Cys397 Tyr435
Cholestane	Cluster 1	0		6	Phe343 Leu328 Ile199 Tyr60 Tyr435 Trp432
3-methoxy-morphanin		0		2	Tyr60 Tyr435

Table 7
Cluster analysis of MD stimulation trajectories of the lead phytochemical-enzyme bond complexes.

Complexes	Number of clusters generated	Size of each cluster,	Representative frame Number	Spread
Cholestane_ *h*AChE	5	1 = 117	71	2.10
		2 = 245	198	1.95
		3 = 179	398	1.85
		4 = 270	771	1.88
		5 = 190	912	1.83
3-methoxy-morphanin_ *h*BChE	2	1 = 308	176	2.22
		2 = 693	789	2.35
Cholestane_ *h*BChE	4	1 = 232	106	2.09
		2 = 230	374	1.95
		3 = 368	711	1.72
		4 = 171	876	1.62
3-methoxy-morphanin_ *h*BChE	4	1 = 210	93	1.95
		2 = 180	344	1.66
		3 = 240	500	1.72
		4 = 371	800	1.63
Cholestane_ MAO-B	4	1 = 41	23	2.11
		2 = 92	74	2.12
		3 = 120	192	1.72
		4 = 273	404	1.63
		5 = 273	787	1.89
3-methoxy-morphanin_ MAO-B	4	1 = 41	23	2.57
		2 = 172	295	1.90
		3 = 342	512	2.06
		4 = 289	836	2.33

Å throughout the period of the simulation (Fig. 11). A maximum fluctuation was observed by the Safinamide bound-MOA B complex. The mean RMSD shows that the binding of 3-methoxy-morphanin reduced the mean RMSD of the three enzymes. The binding 3-methoxy-morphanin to the three proteins enhanced the stability of the proteins. The RMSF plots reveals the flexibility of different regions of the enzymes. For the RMSF plots for *h*AChE, *h*BChE and MAO-B, is presented in Fig. 12. The MAO-B-safinamide system presented higher RMSF fluctuation compared to the other systems. The mean RMSF shows that the binding of 3-methoxy-morphanin reduced the mean RMSF of the three enzymes, indicating that the internal flexibility of the enzymes was not distorted by the binding of the lead phytochemicals. The compactness of the bound systems was further measured from the analysis of the RoG plots. Usually, an increase in the fluctuation indicates a distortion of the folding of the protein. The RoG plots for the hAChE, *h*BChE and MAO-B systems were also equilibrated around 5 ns with minimal fluctuation throughout the period of the simulation (Fig. 13). The MAO-B-safinamide system presented higher RoG fluctuation compared to the other systems. The binding of 3-methoxy-morphanin reduced the fluctuations and mean RoG values in the hAChE, *h*BChE and MAO-B systems, while cholestane reduced the fluctuations and mean RoG values in the *h*BChE and MAO-B systems. The SASA plots reveals the extent of solvent accessibly by the surface of the protein. Both RoG and SAS are used to study if the binding of the ligands affects the integrity of the folded protein. The three enzyme systems presented low fluctuation as observed from the SASA plots (Fig. 14). In the *h*BChE system, the binding of the two lead phytochemicals reduced the mean SASA values. The number of hydrogen bonds during the simulation was fairly constant with minimal fluctuations. The ligand bound-complexes presented

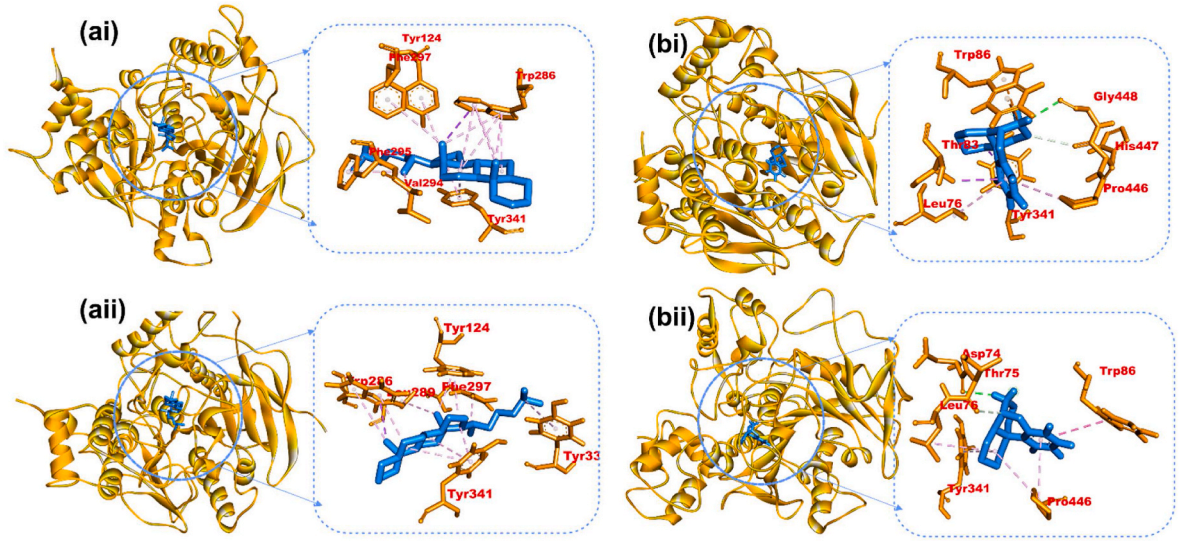


Fig. 17. Amino acid interaction of lead phytochemicals: (a) 3-methoxy-morphanin (b) cholestane in the first cluster (i) and last cluster (ii) of *h*AChE complexes obtained from the cluster analysis of the MDS trajectories.

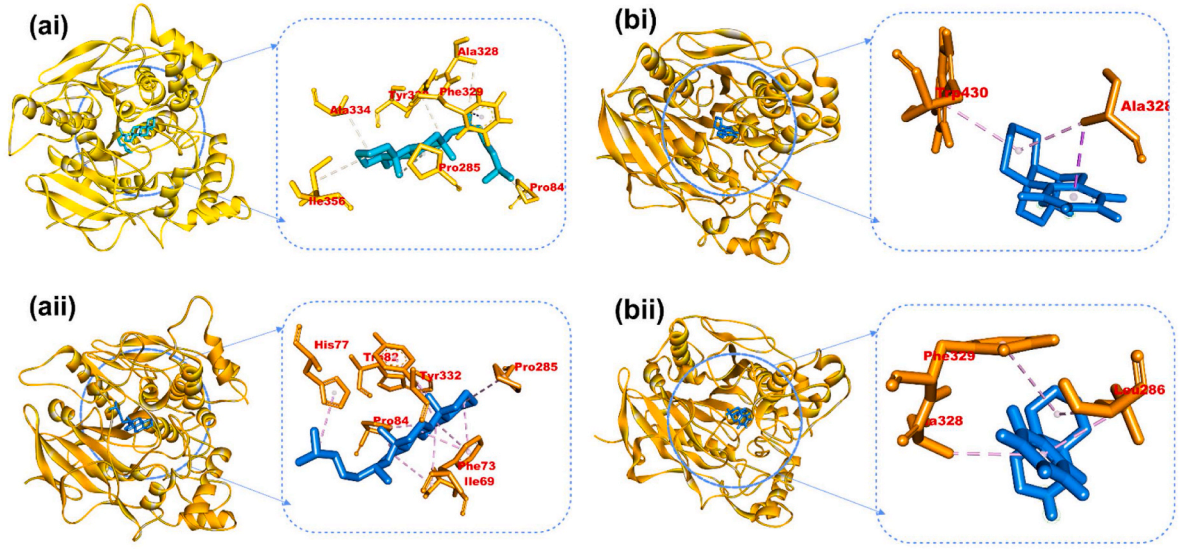


Fig. 18. Amino acid interaction of lead phytochemicals: (a) 3-methoxy-morphanin (b) cholestane in the first cluster (i) and last cluster (ii) of *h*BChE complexes obtained from the cluster analysis of the MDS trajectories.

close number of hydrogen bonds as the apo enzymes (Fig. 15). From the analysis of the various parameters, the 3-methoxy-morphanin bound complexes were more stable compared to the cholestane bound system.

3.3.5. Ensemble-based docking of hit phytocompounds with conformers of AChE, BChE and MAO-B enzyme obtained from the cluster analysis of the MD simulation trajectories

In other to optimize the initial docking procedure, an ensemble docking was done to the representative structures of the various conformers of the human AChE, BChE and MAO-B enzyme that were obtained from the TTClust cluster analysis of the molecular simulation trajectories of a full atomistic 50 ns MD simulation of the apo enzyme. For each of the enzyme the mean and standard error of mean of the binding energies to the different conformer were computed and plotted in Fig. 16. The results of the ensemble-based docking analysis further confirmed cholestane, as the lead phytochemicals with mean binding energies of −9.4343, −9.4667, and −8 kcal/mol for cholestane and −8.8, −8.233, and 7.7 kcal/mol for 3-methoxy-morphanin. When ensemble-based docking was applied the lead compounds presented better binding energy compared to the reference inhibitors. The representative conformer of each cluster with the lowest binding energy for the phytochemicals was selected as the best conformer of the enzyme and further subjected to amino acid interactive analysis. For each of the enzymes, representative structure from cluster 1 had higher binding energy with the phytochemicals. The amino acid interaction of the selected cluster is presented in Table 6. It can be observed that the amino acid interaction with important catalytic residue was preserved in the new conformation. For hAChE, the lead phytochemicals interacted with Trp86 an important residue located in the substrate binding site. For hBChE, interaction with Tyr82 was preserved, while interaction with Tyr435 was preserved in MAO-B (Table 6).

3.3.6. Amino acid interaction of the selected cluster obtained from the cluster analysis of MD simulation trajectories of the lead phytochemical-enzyme bound complexes

After the cluster analysis of the lead phytochemical-enzyme bound

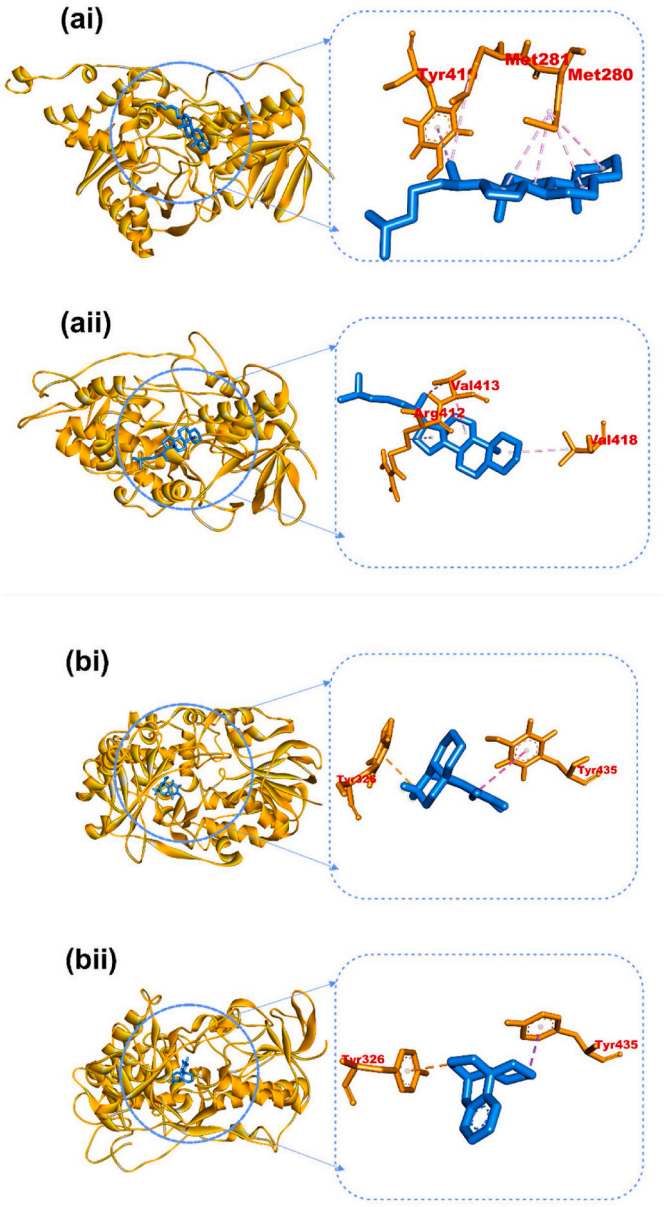


Fig. 19. Amino acid interaction of lead phytochemicals: (a) 3-methoxy-morphanin (b) cholestane in the first cluster (i) and last cluster (ii) of MAO-B complexes obtained from the cluster analysis of the MDS trajectories.

complexes, the number of clusters that were generated from the 1001 frames, the size of the cluster (number of frames that makes up the clusters), the frame number of selected representative cluster and the spread, which is the average distance among the conformations that makes up the cluster is presented in Table 7. The frames that make up each cluster is presented in the supplementary data. The interactions between the amino acid residues of the representative conformations from the clusters, shows that the initial docking interaction obtained from the static docking anlaysis, was preserved during the period of the simulation. It was further observed that the lead phytochemicals we still docked in the substrate binding grove of the enzymes, maintain contact with amino acid of the active sites of the enzymes (Figs. 17–19).

3.3.7. In silico drug-likeness and pharmacokinetic properties of top docked steroidal saponins

The two lead phytochemicals that were gotten from the docking and ensembled-based docking analysis were investigated for predictive drug-likeness and ADMET (Absorption, Distribution, Metabolism, Excretion, and Toxicity) filtering analyses. The results obtained from these analyses are represented in Table 8. From these phytochemicals, cholestane and 3-methoxy-morphanin fulfilled the requirement for at least four from the five physicochemical parameters from the Lipinski rule of five, thereby suggesting favorable druggable properties. Cholestane and 3-methoxy-morphanin presented high gastrointestinal absorption, thereby suggesting high bioavailability. Both phytochemicals presented the ability to cross the brain-blood barrier, which is an important property of neurodegenerative drug (Table 8).

Cholestane and 3-methoxy-morphanin were predicted to be negative substrate of the P-glycoprotein and high plasma protein binding tendencies. The effects of the lead phytochemicals on phase I drug metabolism in the liver was also analysed using a wide range of molecular cytochrome P450 descriptors, the lead phytochemicals are predicted not to present inhibitory potential for the cytochrome P450 descriptors. The predictive analysis further revealed that the lead phytochemicals were

Table 8
In silico Druglikeness and ADMET[a] parameters of the top two docked phytochemicals to human HMG-CoA reductase and xanthine oxidase.

	Cholestane	3-methoxy-morphanin
Molecular weight (g/mol)	372.64	257.37
Num. arom. Heavy atoms	0	6
Num. heavy atoms	27	19
Num. H-bond acceptors	0	2
Num. rotatable bonds	5	1
Hydrogen bond donor	0	1
cLogP	5.16	2.97
Molar Refractivity	122.93	81.58
TPSA (Å^2)	0.00	21.26
Drug-likeness		
Lipinski	Yes (1 violation: MLOGP>4.15	Yes
Veber	Yes	Yes
Bioavailability Score	0.55	0.17
Absorption (Probability)		
(b) Admet SAR		
HIA	HIA+ (1.0)	HIA+ (0.960)
Blood-Brain Barrier	BBB+(0.864)	BBB+(0.988)
P-glycoprotein Substrate	Neg. (0.55334)	Neg. (0.812)
Caco-2 Permeability Cm/s	Caco2+ (0.710)	Caco2+ (0.576)
Distribution (Probability)		
PPB %	90.031	71.37
VD L/kg	1.54.578	1.164.042
Metabolism (Probability)		
CYP450 1A2 Inhibitor	Neg. (0.703)	Neg. (0.799)
CYP450 1A2 Substrate	Neg. (0.408)	Pos. (0.758)
CYP450 3A4 Inhibitor	Neg. (0.918)	Neg. (0.518)
CYP4502C9 Inhibitor	Neg. (0.12)	Neg. (0.907)
CYP450 2C9 Substrate	Neg. (0.861)	Neg. (0.754)
CYP4502C19 Inhibitor	Neg. (0.854)	Neg. (0.735)
CYP450 2C19 Substrate	Neg. (0.412)	Pos. (0.749)
CYP4502D6 Inhibitor	Neg. (0.845)	Pos. (0.552)
CYP450 2D6 Substrate	Neg. (0.488)	Neg. (0.218)
Elimination		
T $_{1/2}$ (Half Life Time)	0.013 h	1.165 h
CL (Clearance Rate) mL/min/kg	13.57	2.551
Toxicity		
hERG Blockers	Neg. (0.58)	Neg. (0.535)
AMES	Neg. (0.907)	Neg. (0.724)
Carcinogen	Neg. (07815)	Neg. (0.965)
SkinSen	Neg (0.264)	Neg (0.235)
LD_{50} (LD_{50} of acute toxicity)	2.923 -log mol/kg (444.978 mg/kg)	2.705 -log mol/kg (507.65 mg/kg)

[a] ADMET: Absorption, distribution, metabolism, elimination, and toxicity; BBB: Blood Brain Barrier; GI: CYP: cytochrome P450; permeability glycoprotein; P-gp: hERG: human Ether-à-go-go-Related Gene; Gastro-intestinal; H-HT: Human Hepatotoxicity AMES; HIA: Human Intestinal Absorption; DILI: Drug Induced Liver Injury; PPB: Plasma Protein Binding; VD: Volume Distribution and Ames Mutagenicity.

not mutagenic and carcinogenic and will not induce skin sensitization. The predicted LD_{50}, half life time and clearance rate of the lead phytochemicals were in acceptable range (Table 8).

4. Discussion

We applied extraction of methanol extract of the leaves, solvent-solvent partitioning of the methanol extract, cholinesterase and mono amine enzyme inhibitory assay, chemical investigation using GC-MS analysis and several computational approaches to identify the potential neurotherapeutic constituent in the leaf of *O. gratissimum*. The concentration-dependent AChE and BChE inhibitory activities of the methanol extract and solvent fractions of the methanol extract of *O. gratissimum* was in agreement with previous studies on the same leave [53]. After considering the IC_{50} of the solvent fractions and analysis to be used for the identification of the chemical constituents in the fraction, the n-hexane fraction was selected for GC-MS analysis. Previous studies have reported the chemical investigation of *O. gratissimum* using GC-MS analysis. Recently Baba et al. [54] reported the GC-MS profiling of ethanol and dichloromethane extracts of the leaves and reported the abundance of decahydro-4a-methyl-1methyl-7-(1-methylethenenyl)-na phthalene, methyl (Z)-5,11,14,17-eicosatetraenoic acid, benzene, tert-butylhydroquinone, 12,15-octadecatrienoic acid, 1-heptatriacotanol, caryophyllene, squalene, phytol acetate, etc.

Selvaraju et al. [55] reported Phytol, Octadecanoic acid, Oleoc acid, Caryophyllene, Clohexene-1-methanol4-[1-methylethenyl]-acetate, Artemisinin, Eugenol, as major compounds. The major identified constituent of the essential oil of *O. gratissimum* have been reported to be eugenol with about 48.4% abundance [56]. The present study performed a GC-MS analysis on the n-hexane partition fraction of the methanol fraction of *O. gratissimum* leaves, selected based on its inhibitory activities. Oleic acid, hexadecanoic acid and thymol were identified as the major constituent, this phytocompounds have been previously reported as major constituents of the leaf [55]. The neuroprotective effect of oleic acid in rat models has been previously documented [57]. Several studies have documented the mitigating activities of monosodium glutamate-induced and 6-hydroxydopamine-induced neurotoxicity [58,59] and neurodegeneration from altered dopaminergic activities in rotenone-Induced rat models [60].

Computer-aided drug discovery tools have been developed as advanced methods for drug discovery, these tools have been applied to screen the potential drug candidates from phytochemicals identified or characterized from several medicinal plant [61]. In this regards, molecular docking, an inexpensive and effective method for investigating the interaction of ligands with known receptors can be employed in predicting the orientation of the potential drug candidate in binding sites of the target protein [19].

In this study, the GC-MS identified phytocompuonds were docked against the hAChE, hBChE and MAO-B enzymes. Result from the initial docking experiment identified seven hit phytochemicals (cholestane, 3-methoxy-morphanin, 2,3,dihydroxyprophlester, oleic acid, hexadecylester, cyclopentaneundecanoic acid and tert-hexadecanethiol with strong binding interactions with the catalytic residues of the 3 enzymes, with cholestane and 3-methoxy-morphanin as the two lead phytochemicals. The neurotherapeutic activity of morphinan compuonds has been reported.

Several *in vitro* cell cultures or studies involving the use of PD animal models have reavealed that morphinan compounds such as dextromethorphan (DM) and metabolites derived from DM have neuroprotective activity as a result of their inhibitory function towards microglia activation and anti-inflammatory properties [62]. A metabolite of DM, 3-Hydroxymorphinan (3-HM) has been reported to be neurotrophic to dopaminergic neurons. 3-HM demostrated neuroprotective activity against LPS-induced neurotoxicity [63]. DM inhibits microglia activation and is neuroprotective when administered daily to mice that had been injected with MPT [63]. In the same study, 3-HM was demostrated the highest potency among the several tested methorphanins, for attenuating the loss of dopamine neurons in the substantia nigra pars compacta, in addition to restoring motor functions in the same MPTP-mouse model of PD [63]. In the same vein, there are report on the neuroprotective activities of compounds with the cholestane core steriodal framework such as with anti-AChE and BChE inhibitory potentials *in vitro* and in vivo studies [64,65].

The respective native ligands with known inhibitory activities against studied enzymes, have provided insight into their catalytic mechanisms, [66–68]. The results from the docking experiment were compared with that of co-crystalized inhibitors of the enzymes. Cholestane and 3-methoxy-morphanin was found accommodated in the long, narrow, hydrophobic gorge of BChE and AChE [67] in comparable binding mode as donepezil. Just as the more complex binding mode of donepezil as compared to other inhibitors these phytochemicals interacted with catalytic residues that makes up the length of the active site gorge of AChE [41]. The aromatic moieties of these phytochemicals interacted via pronounced π-π stacking to the aromatic amino acids especially of peripheral anionic site (P-site) residues that is positioned at the rim of the gorge which offers allosteric and inhibitors a binding site [68]. The lead phytochemicals interacted with the anionic choline-binding site residues (Tyr334, Phe331 and Trp86). Among these aromatic residues Trp86 and Try337 have been reported to be important for the inhibition of the *h*AChE enzyme [69,70]. The variances in the ligand binding specificity between BChE and AChE have been reported to arise from different number of aromatic residues that is situated in the gorge, only 4 of the aromatic residues in the gorge of hAChE are found in the gorge of hBChE. In a similar binding pattern as the decamethonium, Cholestane and 3-methoxy-morphanin was orientated in the gorge, interacted with the amino acid residues of the P-sites Tyr332 (Tyr341 in *h*AChE) and A-sites Phe329, Trp231 and Trp82, (Phe338, Trp236 and Trp86, in *h*AChE). Substrates with positive charge like butyrylcholine are guided down the catalytic gorge through interaction with Tyr 332 and Asp70 which are situated at the lip portion of the *h*BChE active site gorge [71].

Ensemble-based molecular docking approach in which several conformations of the targeted enzymes, usually obtained from MD simulation, has recently been established as a more inadept molecular docking analysis [22]. The result from the ensemble-based molecular docking in which the hit compounds were further docked to several conformers of the respective protein, shows that despite the change in conformation, the lead phytochemicals were able to bind and interact with the active site residues.

The stability of the lead phytochemicals complexed to the enzyme target was further studied through a full atomistic MD simulation. The bound structures were compared to the unbound structures through several analysis on the MD simulation trajectories that was obtained. The RMSD plots reveals the degree of deviation of each frame from the initial structure, therefore it is used to access the stability of the protein systems. The binding of the lead phytochemicals especially 3-methoxy-morphanin enhanced the stability of the complexes [72]. The RMSF plots reveals the flexibility of different regions of the enzymes, The binding of the led phytochemicals did not distort the internal flexibility of the enzymes [73]. The compactness of the bound systems was further measured from the analysis of the RoG plots. Usually, an increase in the fluctuation indicates a distortion of the folding of the protein. The SASA plots reveals the extent of solvent accessibly by the surface of the protein. Both RoG and SAS are used to study if the binding of the ligands affects the integrity of the folded protein [74]. Both analyses showed that compactness of the protein structures were not compromised. Also, the binding of the lead phytochemical did not alter the intra-molecular hydrogen bonds [51,75]. Apart from the stability of the bound complexes, the trajectories of the MD simulation were clustered and representative conformers were further subjected to interaction analysis. It was observed that the interactions observed in the static docking environment (H-bonds and hydrophobic interaction) and ensemble-docking

were maintained at different time frames of the simulation. Further suggesting that the binding interactions reported in this study can be sustained in a more dynamic environment [52]. The result obtained from the use of several ADMET filtering tools suggests a favorable ADMET and pharmacokinetic properties. Using both the Lipinski and Veber filtering tool, Cholestane and 3-methoxy-morphanin fulfilled the requirement as potential drug candidate [76]. Favorable Veber and Lipinski properties specifies good permeation or absorption and good oral bioavailability respectively [77,78]. Among the several in silico descriptors that were studied for toxicity, hERG channel performs an important role in the repolarization and termination stages of action potential in cardiac cell, compounds that inhibits the hERG channel may cause cardiotoxicity. The lead phytochemicals did not display the tendencies of being hERG channel blockers, indicating that they may not cause cardiotoxicity related to the hERG channel [79,80]. Also, using the various cytochrome P450 descriptors the impact of the lead compounds on phase I drug metabolism was analysed. They demonstrated less inhibitory potential for the several cytochrome P450, hence, may not unfavorably affect phase I drug metabolism a large extent [80]. The BBB is known as a barricade protecting the brain via a 'physical' barrier and a 'biochemical' barrier made of enzymatic activities and dynamic efflux [81] that serves as an important fence between the systemic circulation and CNS. This has been one of the greatest problems of CNS drug delivery [82]. Among the several molecular descriptors that was studied in silico, the lead compounds were positive for ability to cross the blood brain barrier (BBB) which further indicates that the compounds can enter the brain cavity, where their neuroprotective function is mostly needed [83]. Therefore, the multi-target inhibitory tendencies of the lead phytochemicals against AChE, BChE and MAO-B coupled with the ability to cross the BBB indicates a promising lead phytochemical that can be applied in the management and treatment of neurodegenerative disease such as AD.

Funding

This research did not receive any funding

Data availability

All data supporting the findings of this study are available within the article and its supplementary materials.

Please state any sources of funding for your research

This research did not receive any specific grant from funding agencies in the public, Commercial or not-for-profit sectors.

Consent

N/A.

Author contribution

Study design: AAN, SOA, GG.
Laboratory work: EOO, AN, SOO, UNO,FMA, OPA
Data analysis; GG, IA, SOA, AA.
Review: All.

Declaration of competing interest

The authors declare that they have no known competing financial interests or personal relationships that could have appeared to influence the work reported in this paper.

Acknowledgement

We sincerely thank Mr. Femi and Joseph Sunday of the Department of Pharmacology and Therapeutics, Faculty of Basic Medical Sciences, College of Health Sciences. University of Ilorin, Ilorin. Nigeria for their assistance in the laboratory.

Appendix A. Supplementary data

Supplementary data to this article can be found online at https://doi.org/10.1016/j.imu.2023.101261.

References

[1] Harms AS, Thome AD, Yan Z, Schonhoff AM, Williams GP, Li X, et al. Peripheral monocyte entry is required for alpha-Synuclein induced inflammation and Neurodegeneration in a model of Parkinson disease. Exp Neurol 2018;300:179–87.
[2] Enciu AM, Nicolescu MI, Manole CG, Mureşanu DF, Popescu LM, Popescu BO. Neuroregeneration in neurodegenerative disorders. BMC Neurol 2011;11:1–7.
[3] Prado-Prado F, García I. Review of theoretical studies for prediction of neurodegenerative inhibitors. Mini Rev Med Chem 2012;12:452–66.
[4] Majd S, Power JH, Grantham HJ. Neuronal response in Alzheimer's and Parkinson's disease: the effect of toxic proteins on intracellular pathways. BMC Neurosci 2015;16:1–13.
[5] Lakey-Beitia J, Berrocal R, Rao K, Durant AA. Polyphenols as therapeutic molecules in Alzheimer's disease through modulating amyloid pathways. Mol Neurobiol 2015;51:466–79.
[6] Guerrero E, Vasudevaraju P, Hegde ML, Britton G, Rao K. Recent advances in α-synuclein functions, advanced glycation, and toxicity: implications for Parkinson's disease. Mol Neurobiol 2013;47:525–36.
[7] Hampel H, Mesulam M-M, Cuello AC, Farlow MR, Giacobini E, Grossberg GT, et al. The cholinergic system in the pathophysiology and treatment of Alzheimer's disease. Brain 2018;141:1917–33.
[8] Craig LA, Hong NS, McDonald RJ. Revisiting the cholinergic hypothesis in the development of Alzheimer's disease. Neurosci Biobehav Rev 2011;35:1397–409.
[9] Finberg JP, Rabey JM. Inhibitors of MAO B-A and MAO B-B in psychiatry and neurology. Front Pharmacol 2016;7:340.
[10] Behl T, Kaur D, Sehgal A, Singh S, Sharma N, Zengin G, et al. Role of monoamine oxidase activity in Alzheimer's disease: an insight into the therapeutic potential of inhibitors. Molecules 2021;26:3724.
[11] Ademosun AO, Oboh G. Comparison of the inhibition of monoamine oxidase and butyrylcholinesterase activities by infusions from green tea and some citrus peels. Int J Alzheimer's Dis 2014;2014.
[12] Ballard C. Advances in the treatment of Alzheimer's disease: benefits of dual cholinesterase inhibition. Eur Neurol 2002;47:64–70.
[13] Pandey MM, Rastogi S, Rawat A. Indian herbal drug for general healthcare: an overview. Internet J Alternative Med 2008;6:3.
[14] Keskes H, Belhadj S, Jlail L, El Feki A, Damak M, Sayadi S, et al. LC-MS–MS and GC-MS analyses of biologically active extracts and fractions from Tunisian Juniperus phoenice leaves. Pharmaceut Biol 2017;55:88–95.
[15] Yadav R, Khare R, Singhal A. Qualitative phytochemical screening of some selected medicinal plants of shivpuri district (mp). Int J Life Sci Sci Res 2017;3:844–7.
[16] Ugbogu EA, Nwoku CD, Ude VC, Emmanuel O. Evaluating bioactive constituents and toxicological effects of aqueous extract of fermented Pentaclethra macrophylla seeds in rats. Avicenna Journal of Phytomedicine 2020;10:101.
[17] Razack S, Hemanth Kumar K, Nallamuthu I, Naika M, Khanum F. Antioxidant, biomolecule oxidation protective activities of Nardostachys jatamansi DC and its phytochemical analysis by RP-HPLC and GC-MS. Antioxidants 2015;4:185–203.
[18] Yu W, MacKerell AD. Computer-aided drug design methods. Antibiotics: methods and protocols. 2017. p. 85–106.
[19] Lee K, Kim D. In-silico molecular binding prediction for human drug targets using deep neural multi-task learning. Genes 2019;10:906.
[20] Halperin I, Ma B, Wolfson H, Nussinov R. Principles of docking: an overview of search algorithms and a guide to scoring functions. Proteins: Struct, Funct, Bioinf 2002;47:409–43.
[21] Abbas SQ, Ali F, Ishaq M, Bano I, Hassan M, Jin H-Z, et al. A Comprehensive in silico exploration of pharmacological properties, bioactivities, molecular docking, and anticancer potential of vieloplain F from Xylopia vielana Targeting B-Raf Kinase. Molecules 2022;27:917.
[22] Amaro RE, Baudry J, Chodera J, Demir Ö, McCammon JA, Miao Y, et al. Ensemble docking in drug discovery. Biophys J 2018;114:2271–8.
[23] D'Onofrio G, Nabavi SM, Sancarlo D, Greco A, Pieretti S. Crocus sativus L. (Saffron) in alzheimer's disease treatment: bioactive effects on cognitive impairment. Curr Neuropharmacol 2021;19:1606–16. https://doi.org/10.2174/1570159x19666210113144703.
[24] Hannan MA, Rahman MA, Sohag AA, Uddin MJ, Dash R, Sikder MH, et al. Black cumin (Nigella sativa L.): a comprehensive review on phytochemistry, Health benefits, molecular Pharmacology, and safety. Nutrients 2021;13. https://doi.org/10.3390/nu13061784.
[25] Mima Y, Izumo N, Chen J-R, Yang S-C, Furukawa M, Watanabe Y. Effects of Coriandrum sativum seed extract on aging-induced memory impairment in Samp8 mice. Nutrients 2020;12. https://doi.org/10.3390/nu12020455.

[26] Khazdair MR, Anaeigoudari A, Hashemzehi M, Mohebbati R. Neuroprotective potency of some spice herbs, a literature review. J Tradit Complement Med 2019;9:98–105. https://doi.org/10.1016/j.jtcme.2018.01.002.

[27] Patil SM, Ramu R, Shirahatti PS, Shivamallu C, Amachawadi RG. A systematic review on ethnopharmacology, phytochemistry and pharmacological aspects of Thymus vulgaris Linn. Heliyon 2021;7:e07054. https://doi.org/10.1016/j.heliyon.2021.e07054.

[28] Eskandari-Roozbahani N, Shomali T, Taherianfard M. Neuroprotective effect of Zataria multiflora essential oil on rats with alzheimer disease: a mechanistic study. BCN 2019;10:85–97. https://doi.org/10.32598/bcn.9.10.270.

[29] Ojo OA, Okesola MA, Ekakitie LI, Ajiboye BO, Oyinloye BE, Agboinghale PE, et al. Gongronema latifolium Benth. leaf extract attenuates diabetes-induced neuropathy via inhibition of cognitive, oxidative stress and inflammatory response. J Sci Food Agric 2020. https://doi.org/10.1002/jsfa.10491. n/a.

[30] Yuan H, Ma Q, Ye L, Piao G. The traditional medicine and modern medicine from natural products. Molecules 2016;21:559.

[31] Bora KS, Shri R, Monga J. Cerebroprotective effect of Ocimum gratissimum against focal ischemia and reperfusion-induced cerebral injury. Pharm Biol 2011;49:175–81. https://doi.org/10.3109/13880209.2010.506489.

[32] Udi OA, Oyem JC, Ebeye OA, Chris-Ozoko LE, Igbigbi PS, Olannye DU. The effects of aqueous extract of ocimum gratissimum on the cerebellum of male wistar rats challenged by lead acetate. Clinical Nutrition Open Science 2022;44:28–41.

[33] Owokotomo IA, Ekundayo O, Abayomi TG, Chukwuka AV. In-vitro anti-cholinesterase activity of essential oil from four tropical medicinal plants. Toxicol Rep 2015;2:850–7. https://doi.org/10.1016/j.toxrep.2015.05.003.

[34] Owokotomo I, Ekundayo O, Abayomi T, Chukwuka A. In-vitro anti-cholinesterase activity of essential oil from four tropical medicinal plants. Toxicol Rep 2015;2:850–7.

[35] Kobenan KC, Bini KKN, Kouakou M, Kouadio IS, Zengin G, Ochou GEC, et al. Chemical composition and spectrum of insecticidal activity of the essential oils of ocimum gratissimum L. And cymbopogon citratus stapf on the main insects of the cotton entomofauna in côte d'Ivoire. Chem Biodivers 2021;18:e2100497.

[36] Harbone J. Phytochemical Analysis–A guide to modern techniques of plant analysis. New York: Chapman & Hall; 1980.

[37] Ellman GL, Courtney KD, Andres Jr V, Featherstone RM. A new and rapid colorimetric determination of acetylcholinesterase activity. Biochem Pharmacol 1961;7:88–95.

[38] Perry NS, Houghton PJ, Theobald A, Jenner P, Perry EK. In-vitro inhibition of human erythrocyte acetylcholinesterase by Salvia lavandulaefolia essential oil and constituent terpenes. J Pharm Pharmacol 2000;52:895–902.

[39] Turski W, Turska E, Gross-Bellard M. Modification of the spectrophotometric method of the determination of monoamine oxidase. Enzyme 1972;14:211–20.

[40] Lawal B, Shittu OK, AbdulRasheed-Adeleke T, Ossai PC, Ibrahim AM. GC-MS determination of bioactive constituents of giant African Snail (Archachatina maginata) Haemolymph. 2015.

[41] Cheung J, Rudolph MJ, Burshteyn F, Cassidy MS, Gary EN, Love J, et al. Structures of human acetylcholinesterase in complex with pharmacologically important ligands. J Med Chem 2012;55:10282–6.

[42] Rosenberry TL, Brazzolotto X, Macdonald IR, Wandhammer M, Trovaslet-Leroy M, Darvesh S, et al. Comparison of the binding of reversible inhibitors to human butyrylcholinesterase and acetylcholinesterase: a crystallographic, kinetic and calorimetric study. Molecules 2017;22:2098.

[43] Binda C, Wang J, Pisani L, Caccia C, Carotti A, Salvati P, et al. Structures of human monoamine oxidase B complexes with selective noncovalent inhibitors: safinamide and coumarin analogs. J Med Chem 2007;50:5848–52.

[44] Trott O, Olson AJ. AutoDock Vina: improving the speed and accuracy of docking with a new scoring function, efficient optimization, and multithreading. J Comput Chem 2010;31:455–61.

[45] O'Boyle NBanck M, James Ca Morley C, Vandermeersch T, Hutchison GR. Open Babel: an open chemical toolbox. J Cheminf 2011;3:33.

[46] Abraham MJ, Murtola T, Schulz R, Páll S, Smith JC, Hess B, et al. GROMACS: high performance molecular simulations through multi-level parallelism from laptops to supercomputers. SoftwareX 2015;1:19–25.

[47] Gromacs-a parallel computer for molecular-dynamics simulations. In: Bekker H, Berendsen H, Dijkstra E, Achterop S, Vondrumen R, Vanderspoel D, et al., editors. 4th international conference on computational physics (PC 92). World Scientific Publishing; 1993.

[48] Oostenbrink C, Villa A, Mark AE, Van Gunsteren WF. A biomolecular force field based on the free enthalpy of hydration and solvation: the GROMOS force-field parameter sets 53A5 and 53A6. J Comput Chem 2004;25:1656–76.

[49] Humphrey W, Dalke A, Schulten K. VMD: visual molecular dynamics. J Mol Graph 1996;14:33–8.

[50] Tubiana T, Carvaillo J-C, Boulard Y, Bressanelli S. TTClust: a versatile molecular simulation trajectory clustering program with graphical summaries. J Chem Inf Model 2018;58:2178–82.

[51] Ogunyemi OM, Gyebi GA, Elfiky AA, Afolabi SO, Ogunro OB, Adegunloye AP, et al. Alkaloids and flavonoids from African phytochemicals as potential inhibitors of SARS-Cov-2 RNA-dependent RNA polymerase: an in silico perspective. Antiviral Chem Chemother 2020;28:2040206620984076.

[52] Ogunyemi OM, Gyebi GA, Ibrahim IM, Olaiya CO, Ocheje JO, Fabusiwa MM, et al. Dietary stigmastane-type saponins as promising dual-target directed inhibitors of SARS-CoV-2 proteases: a structure-based screening. RSC Adv 2021;11:33380–98.

[53] Owokotomo IA, Ekundayo O, Abayomi TG, Chukwuka AV. In-vitro anti-cholinesterase activity of essential oil from four tropical medicinal plants. Toxicol Rep 2015;2:850–7. https://doi.org/10.1016/j.toxrep.2015.05.003.

[54] Baba H, Kashimawo AJ, Ibe AC. Phytochemical evaluation and GC-MS profiling of the dichloromethane and ethanol extracts of Ocimum gratissimum L. and Lasianthera Africana. BEAUV. Journal of Phytomedicine and Therapeutics 2022;20:640–55.

[55] Selvaraju R, Sakuntala P, Jaleeli K. GC–MS and FTIR analysis of chemical compounds in Ocimum gratissimum plant. Biophysics 2021;66:401–8.

[56] Unnithan C, Sushen U. Chemical composition of Ocimum gratissimum L by GC-MS analysis. Eur J Pharm Med Res 2017;4:410–2.

[57] Song J, Kim Y-S, Lee DH, Lee SH, Park HJ, Lee D, et al. Neuroprotective effects of oleic acid in rodent models of cerebral ischaemia. Sci Rep 2019;9:10732.

[58] Mostafa R, Hassan A, Salama A. Thymol mitigates monosodium glutamate-induced neurotoxic cerebral and hippocampal injury in rats through overexpression of nuclear erythroid 2-related factor 2 signaling pathway as well as altering nuclear factor-kappa b and glial fibrillary acidic protein expression. Open Access Maced J Med Sci 2021;9:716–26.

[59] Nourmohammadi S, Yousefi S, Manouchehrabadi M, Farhadi M, Azizi Z, Torkaman-Boutorabi A. Thymol protects against 6-hydroxydopamine-induced neurotoxicity in in vivo and in vitro model of Parkinson's disease via inhibiting oxidative stress. BMC Complement Med Therap 2022;22:1–14.

[60] Javed H, Azimullah S, Meeran MN, Ansari SA, Ojha S. Neuroprotective effects of thymol, a dietary monoterpene against dopaminergic neurodegeneration in rotenone-induced rat model of Parkinson's disease. Int J Mol Sci 2019;20:1538.

[61] Sliwoski G, Kothiwale S, Meiler J, Lowe EW. Computational methods in drug discovery. Pharmacol Rev 2014;66:334–95.

[62] Liu Y, Qin L, Li G, Zhang W, An L, Liu B, et al. Dextromethorphan protects dopaminergic neurons against inflammation-mediated degeneration through inhibition of microglial activation. J Pharmacol Exp Therapeut 2003;305:212–8.

[63] Zhang W, Wang T, Qin L, Gao HM, Wilson B, Ali SF, et al. Neuroprotective effect of dextromethorphan in the MPTP Parkinson's disease model: role of NADPH oxidase. Faseb J 2004;18:589–91.

[64] Ayaz M, Junaid M, Ullah F, Subhan F, Sadiq A, Ali G, et al. Anti-Alzheimer's studies on β-sitosterol isolated from Polygonum hydropiper L. Front Pharmacol 2017;8:697.

[65] Wu Bari, Zahoor M, Zeb A, Khan I, Nazir Y, Khan A, et al. Anticholinesterase, antioxidant potentials, and molecular docking studies of isolated bioactive compounds from Grewia optiva. Int J Food Prop 2019;22:1386–96.

[66] Harel M, Schalk I, Ehret-Sabatier L, Bouet F, Goeldner M, Hirth C, et al. Quaternary ligand binding to aromatic residues in the active-site gorge of acetylcholinesterase. Proc Natl Acad Sci USA 1993;90:9031–5.

[67] Silman I, Harel M, Axelsen P, Raves M, Sussman JL. Three-dimensional structures of acetylcholinesterase and of its complexes with anticholinesterase agents. Biochem Soc Trans 1994;22:745–9.

[68] Sussman JL, Harel M, Frolow F, Oefner C, Goldman A, Toker L, et al. Atomic structure of acetylcholinesterase from Torpedo californica: a prototypic acetylcholine-binding protein. Science 1991;253:872–9.

[69] Ashani Y, Grunwald J, Kronman C, Velan B, Shafferman A. Role of tyrosine 337 in the binding of huperzine A to the active site of human acetylcholinesterase. Mol Pharmacol 1994;45:555–60.

[70] Harel M, Schalk I, Ehret-Sabatier L, Bouet F, Goeldner M, Hirth C, et al. Quaternary ligand binding to aromatic residues in the active-site gorge of acetylcholinesterase. Proc Natl Acad Sci U S A 1993;90:9031–5. https://doi.org/10.1073/pnas.90.19.9031.

[71] Darvesh S, Hopkins DA, Geula C. Neurobiology of butyrylcholinesterase. Nat Rev Neurosci 2003;4:131–8. https://doi.org/10.1038/nrn1035.

[72] Cheng X, Ivanov I. Molecular dynamics. Computat Toxicol 2012;ume I:243–85.

[73] Dong Y-w, Liao M-l, Meng X-l, Somero GN. Structural flexibility and protein adaptation to temperature: molecular dynamics analysis of malate dehydrogenases of marine molluscs. Proc Natl Acad Sci USA 2018;115:1274–9.

[74] Sinha S, Wang SM. Classification of VUS and unclassified variants in BRCA1 BRCT repeats by molecular dynamics simulation. Comput Struct Biotechnol J 2020;18:723–36.

[75] Gyebi GA, Ogunyemi OM, Ibrahim IM, Ogunro OB, Adegunloye AP, Afolabi SO. SARS-CoV-2 host cell entry: an in silico investigation of potential inhibitory roles of terpenoids. J Genetic Eng Biotechnol 2021;19:1–22.

[76] Daina A, Michielin O, Zoete V. SwissADME: a free web tool to evaluate pharmacokinetics, drug-likeness and medicinal chemistry friendliness of small molecules. Sci Rep 2017;7:42717.

[77] Veber DF, Johnson SR, Cheng H-Y, Smith BR, Ward KW, Kopple KD. Molecular properties that influence the oral bioavailability of drug candidates. J Med Chem 2002;45:2615–23.

[78] Lipinski CA. Drug-like properties and the causes of poor solubility and poor permeability. J Pharmacol Toxicol Methods 2000;44:235–49.

[79] Raschi E, Vasina V, Poluzzi E, De Ponti F. The hERG K+ channel: target and antitarget strategies in drug development. Pharmacol Res 2008;57:181–95.

[80] Kratz JM, Grienke U, Scheel O, Mann SA, Rollinger JM. Natural products modulating the hERG channel: heartaches and hope. Nat Prod Rep 2017;34:957–80.

[81] Daina A, Zoete V. A boiled-egg to predict gastrointestinal absorption and brain penetration of small molecules. ChemMedChem 2016;11:1117–21.

[82] Sapkota K, Mao BZ, Synowicki P, Lieber D, Liu M, Ikezu T, et al. GluN2D N-methyl-d-aspartate receptor subunit contribution to the stimulation of brain activity and gamma oscillations by ketamine: implications for schizophrenia. J Pharmacol Exp Therapeut 2016;356:702–11.

[83] Pardridge WM. Alzheimer's disease drug development and the problem of the blood-brain barrier. Alzheimer's Dementia 2009;5:427–32.